

Residues Neighboring an SH3-Binding Motif Participate in the Interaction *In Vivo*

David F. Jordan^{1,2,3,4,*}, Alexandre K. Dubé^{1,2,3,4,5}, Ugo Dionne^{2,3,4,6,7,8}, David Bradley^{1,2,3,4,5} and Christian R. Landry^{1,2,3,4,5,*}

1. Département de Biochimie, microbiologie et bio-informatique, Université Laval, 1045 Avenue de la Médecine, Québec, QC, Canada, G1V 0A6

2. Institut de Biologie Intégrative et des Systèmes (IBIS), 1030, Avenue de la Médecine, Université Laval, Québec, QC, Canada, G1V 0A6

3. PROTEO-Regroupement Québécois de Recherche sur la Fonction, l'Ingénierie et les Applications des Protéines, Université Laval, 1030, Avenue de la Médecine Québec, QC, Canada, G1V 0A6

4. Centre de Recherche en Données Massives de l'Université Laval, Université Laval, 1065, Avenue de la Médecine, Québec, QC, Canada, G1V 0A6

5. Département de Biologie, Université Laval, 1045 Avenue de la Médecine, Québec, QC, Canada, G1V 0A6

6. Centre de Recherche du Centre Hospitalier Universitaire (CHU) de Québec-Université Laval, 11, côte du Palais, Québec, QC, Canada, G1R 2J6

7. Centre de Recherche sur le Cancer de l'Université Laval, 9, rue McMahon, Québec, QC, Canada, G1R 3S3

8. Present address: Lunenfeld-Tanenbaum Research Institute, Sinai Health, 600 University Avenue, Toronto, ON, Canada, M5G 1X5

* Correspondance: 1030, Avenue de la Médecine, Université Laval, Québec, QC, Canada, G1V 0A6 Email: david.jordan.2@ulaval.ca.

1030, Avenue de la Médecine, Université Laval, Québec, QC, Canada, G1V 0A6 Email: christian.landry@bio.ulaval.ca

Running head: Residues neighboring motif participate in interaction

Keywords: Short Linear motif, Src Homology 3 (SH3) domain, Deep mutational scanning, Binding affinity, Structure prediction

35

36 Abstract

37

38 In signaling networks, protein-protein interactions are often mediated by modular domains that
39 bind short linear motifs. The motifs' sequences affect many factors, among them affinity and
40 specificity, or the ability to bind strongly and to bind the appropriate partners. Using Deep
41 Mutational Scanning to create a mutant library, and protein complementation assays to measure
42 protein-protein interactions, we determined the *in vivo* binding strength of a library of mutants of
43 a binding motif on the MAP kinase kinase Pbs2, which binds the SH3 domain of the osmosensor
44 protein Sho1 in *Saccharomyces cerevisiae*. These measurements were made using the full-length
45 endogenous proteins, in their native cellular environment. We find that along with residues within
46 the canonical motif, many mutations in the residues neighboring the motif also modulate binding
47 strength. Interestingly, all Pbs2 mutations which increase affinity are situated outside of the Pbs2
48 region that interacts with the canonical SH3 binding pocket, suggesting that other surfaces on
49 Sho1 contribute to binding. We use predicted structures to hypothesize a model of binding which
50 involves residues neighboring the canonical Pbs2 motif binding outside of the canonical SH3
51 binding pocket. We compared this predicted structure with known structures of SH3 domains
52 binding peptides through residues outside of the motif, and put forth possible mechanisms through
53 which Pbs2 can bind specifically to Sho1. We propose that for certain SH3 domain-motif pairs,
54 affinity and specificity are determined by a broader range of sequences than what has previously
55 been considered, potentially allowing easier differentiation between otherwise similar partners.

56 Summary

57

58 Protein-protein interactions are often mediated by a binding domain on one protein and a short
59 disordered binding motif on another protein. We measured the binding strength of a mutant library
60 of a binding motif situated in the yeast protein Pbs2 to the SH3 domain of Sho1. Many mutations
61 in the residues neighboring the binding motif affect binding. A protein structure prediction of the
62 interaction partners shows that residues neighboring the motif bind residues outside the known
63 binding pocket on the SH3 domain. The Sho1-Pbs2 interaction differs enough from other known
64 SH3-motif pairs to allow specific binding.

65

66

67

68

69

70 Introduction

71 Cells possess complex and robust signaling networks that detect stimuli and trigger responses.
72 These signaling networks are composed of a series of protein-protein interactions, which are often
73 mediated by modular interaction domains. Many classes of protein interaction domains are shared
74 across pathways and species, yet fulfill different roles and functions (Pawson *et al.* 2002). The
75 different constraints placed on interaction domains by their distinct roles contribute to explaining
76 the divergence in sequence between homologs of the same domain (Ernst *et al.* 2010; Dionne *et*
77 *al.* 2022). Therefore, to understand how domain sequences have evolved and continue to evolve,
78 the phenotypic consequences of mutations must be understood. Two of the major phenotypes for
79 protein-protein interaction domains are affinity, that is, the strength of binding to the partner
80 protein, and specificity, that is, the ability to bind to the appropriate partner proteins, and to not
81 form spurious interactions with other proteins in the cellular environment (Ivarsson and Jemth
82 2019).

83
84 Many interaction domains bind short intrinsically disordered stretches of their interaction partners,
85 also known as short linear motifs (SLiMs) or simply binding motifs (Gouw *et al.* 2018). Binding
86 motifs are involved in a wide swath of cell signaling pathways, and underlie many important
87 mechanisms in human and other cells (Kumar *et al.* 2024). Uncovering the determinants of
88 binding can elucidate the functioning of human cells and certain diseases that affect them, such
89 as various cancers in which motif-mediated signaling plays a part (Van Roey *et al.* 2014).
90 Additionally, viruses also use their own binding motifs to disrupt the signaling machinery of their
91 hosts (Davey *et al.* 2011). Understanding domain-motif binding can also allow them to be used
92 as tools, for example by attaching therapeutic proteins to domains and motifs to hydrogels, to
93 ensure the gradual release of the therapeutic proteins in human tissues (Delplace *et al.* 2019).

94
95 Interactions mediated by domain-motif associations are relatively weak, with dissociation
96 constants (K_D) in the micromolar range, while domain-domain binding typically results in
97 dissociation constants values orders of magnitude smaller, indicating much stronger binding (Van
98 Roey *et al.* 2014). While such low affinity could simply be caused by physical limitations, such as
99 the smaller interface, adaptive hypotheses have been put forward which suggest that an overly
100 strong affinity can have deleterious effects on the cell, for instance by compromising specificity
101 (Haslam and Shields 2012; Karlsson *et al.* 2016). Alternatively, this low intrinsic affinity can be
102 compensated by other factors. For example, certain protein-protein interactions depend on the
103 simultaneous binding of many domain-motif pairs (Liao *et al.* 2020). In other cases, motifs bind
104 outside of the canonical binding pockets of their partner domains, although this does not always
105 lead to increased affinity (Douangamath *et al.* 2002). The regions surrounding a domain can also
106 have an effect on motif binding preference, as inserting domains into new protein backgrounds
107 can change the motifs that this domain binds to (Dionne *et al.* 2021, 2022).

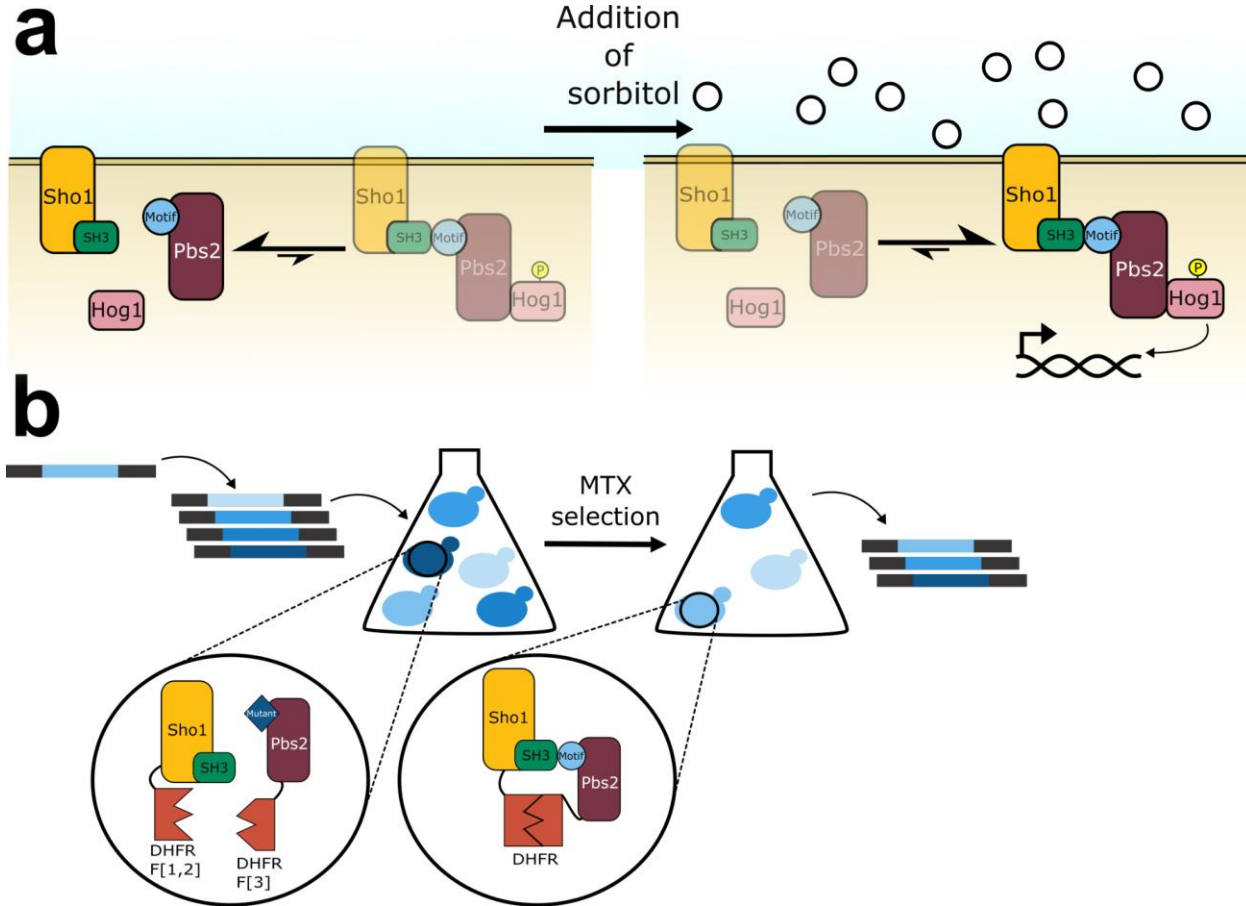
108
109 Binding affinity and specificity have previously been explored in the context of the interaction
110 between binding domains and motifs, by measuring the binding of mutants *in vitro* (Yu *et al.* 1994;
111 Zarrinpar *et al.* 2003; Tonikian *et al.* 2009; Vincentelli *et al.* 2015; Kazlauskas *et al.* 2016).
112 However, the interaction of proteins in the cellular environment is a more complex situation, and

113 many interactions detected *in vivo* are not detected *in vitro*, and vice versa (Kelil *et al.* 2017).
114 Many factors can modulate binding in the cell, including colocalization of partners, expression in
115 the same cell cycle phases, and contributions from sequences outside of the immediate binding
116 domain and motif, as well as other proteins that can interact with one or both of the partners
117 (Ivarsson and Jemth 2019; Dionne *et al.* 2022). Earlier studies have measured the effects of
118 limited numbers of domain and motif mutants *in vivo* (Zarrinpar *et al.* 2003; Marles *et al.* 2004).
119 More recently, techniques such as deep mutational scanning (DMS) have been used to study the
120 impact of large libraries of mutations on protein stability and function *in vivo* (Fowler and Fields
121 2014). Methods such as protein complementation assays (Tarassov *et al.* 2008; Michnick *et al.*
122 2016) have also successfully been used to measure the *in vivo* binding strength of libraries of
123 mutants in yeast (Diss and Lehner 2018; Dionne *et al.* 2021; Faure *et al.* 2022; Robles *et al.* 2023;
124 Dibyachintan *et al.* 2024; Bendel *et al.* 2024). For example, a recent study showed the effect on
125 binding of combining mutations in a PDZ domain and its binding motif (Zarin and Lehner 2024).
126 These *in vivo* techniques could be used to determine how a large library of mutations can affect
127 domain-motif interaction affinity.
128

129 One powerful model to study domain-motif interactions is SH3 domains. These globular domains
130 are composed of around 60 residues, and bind different classes of proline-rich motifs defined by
131 the canonical forms R/KXXPXXP for class I and PXXPXR/K for class II (Kaneko *et al.* 2008). The
132 model yeast *Saccharomyces cerevisiae*'s proteome contains 27 different SH3 domains (Dionne
133 *et al.* 2022), including one in the High Osmolarity Glycerol (HOG) signaling pathway protein Sho1
134 (Saito and Posas 2012). The SH3 domain of Sho1 is known to interact with a motif on the MAPKK
135 Pbs2, and this interaction can be strengthened by exposing cells to osmotic stress (Maeda *et al.*
136 1995; Posas and Saito 1997; Saito and Posas 2012) (Figure 1a). The Sho1-Pbs2 interaction is
137 thus a powerful model to study domain-motif interaction strength, due to the potential for
138 increasing or decreasing affinity through mutations and the simple method of inducing an increase
139 in the interaction strength using osmotic stress.
140

141 To better understand the impact of mutations on affinity, we measured the binding strength of a
142 nearly complete library of mutations in the Pbs2 binding motif *in vivo* using a DHFR Protein-
143 fragment Complementation Assay (PCA) (Tarassov *et al.* 2008; Michnick *et al.* 2016). We
144 measured the binding strength between single residue Pbs2 motif mutants and Sho1, the
145 canonical partner of Pbs2. We find that all single mutations that increase the interaction strength
146 are found outside the canonical binding motif, and that certain residues outside the binding motif
147 are predicted to interact with Sho1 outside of the canonical binding pocket, and even outside of
148 the SH3 domain. We use this finding to propose a model of Sho1-Pbs2 binding, where residues
149 outside the canonical Pbs2 motif bind a second binding pocket on Sho1. We also compare this
150 proposed model to other known SH3-motif interactions involving binding outside the canonical
151 motif.
152
153
154
155
156

157
158



159
160

161 **Figure 1. The Sho1-Pbs2 interaction can be strengthened using sorbitol exposure, and the DHFR-**
162 **PCA can be used to measure the interaction strength between Sho1 and Pbs2.**

163 a) Simplified schematic of the HOG pathway, and the interactions between Sho1, Pbs2 and
164 Hog1. In normal conditions (left), Sho1, Pbs2 and Hog1 are mostly separated. In the presence of
165 osmotic stress such as sorbitol (right), signaling through the pathway is induced, the proteins
166 assemble into a complex, and Hog1 is phosphorylated, which causes it to modulate gene
167 expression via translocation to the nucleus. b) Schematic of the DHFR-PCA screen with a DMS
168 mutant library. Single residue variants of PBS2 were inserted into the yeast genome at the native
169 locus using CRISPR-Cas9 genome editing. Sho1 and Pbs2 were tagged with complementary
170 DHFR fragments. In cases where the Pbs2 variant does not interact with Sho1, the DHFR
171 fragments remain separated. Upon interaction between a Pbs2 variant and Sho1, the DHFR
172 fragments combine to reconstitute the functional DHFR, and allow growth in the presence of
173 methotrexate (MTX). More strongly interacting partners allow the cell to proliferate more rapidly
174 (Freschi *et al.* 2013).

175

176 Results

177 Scan of the region surrounding the Pbs2 motif reveals that few mutations modify binding to Sho1

178 The interaction between Sho1 and Pbs2 is modulated by an SH3 domain on Sho1 and the
179 canonical binding motif on Pbs2, which is a type I motif with the sequence KPLPPLP (Maeda *et*
180 *al.* 1995). Previous computational work has suggested that the region surrounding binding motifs
181 could play an important role in modulating binding, including in SH3 interactions and in particular
182 in the Sho1-Pbs2 interaction (Stein and Aloy 2008; Kelil *et al.* 2016). To determine which Pbs2
183 residues play a role in binding, we undertook a Deep Mutational Scan (DMS) on a region of 56
184 codons comprising the binding motif and its surrounding region. A DNA library of every possible
185 single codon mutant was created for the 56 codon stretch, and inserted into the *S. cerevisiae*
186 genome at the PBS2 locus using a CRISPR Cas-9 based approach, replacing the wild-type
187 sequence (Dionne *et al.* 2021). The *PBS2* gene was fused with a Dihydrofolate Reductase
188 Protein-Fragment 3 (DHFR F[3]), and these cells were mated with cells containing a DHFR F[1,2]
189 fusion with *SHO1*, in order to obtain diploid strains containing complementary DHFR fusions on
190 both interaction partners. An interaction between Sho1 and Pbs2 brings the two DHFR fragments
191 into contact, forming a functional DHFR which allows cell division even in the presence of the
192 drug methotrexate (MTX) (Figure 1b). Growth in the presence of MTX in a strain with both DHFR
193 fragments is therefore a proxy for the amount of Sho1-Pbs2 complexes forming, which depends
194 on both the binding affinity and the local abundance of the interacting proteins (Tarassov *et al.*
195 2008; Freschi *et al.* 2013). As the DHFR fusions are located at the C-terminus of proteins,
196 nonsense mutations introduced in the mutant library lead to no DHFR fragment expression.
197

198 To measure the interaction strength of the DMS library, the mutants were pooled and DHFR-PCA
199 competition assays were done in media containing both MTX and 1 M of sorbitol, in order to
200 induce the HOG pathway (Ferrigno *et al.* 1998). The resulting interaction score was calculated as
201 the normalization of log-2-fold change of variant frequencies before and after selection for the
202 interaction using MTX, as detected by targeted sequencing of the *PBS2* locus. Interaction scores
203 were normalized in each replicate, so that scores of 0 are equivalent to wild-type Pbs2, while
204 interaction scores of -1 correspond to the median of all nonsense mutants. Mutants which possess
205 a higher interaction strength than wild-type Pbs2 therefore have a positive interaction score, while
206 mutants which possess a lower interaction score than wild-type Pbs2 have a negative interaction
207 score.
208

209 Many mutations in the canonical motif change the interaction strength. However, we found that
210 most mutations in the region surrounding the motif did not affect binding of Sho1, apart from a
211 short section neighboring the canonical motif itself (Figure 2a, Figure S1, Figure S2, Table S1).
212 This confirms the strong role of the motif in the interaction and validates the computational
213 predictions that extended the role of binding to include neighboring residues (Stein and Aloy 2008;
214 Kelil *et al.* 2016). Since the effect on binding was strongly position dependent, we categorized
215 different sections of Pbs2 as follows: the canonical binding motif is the conserved type I binding
216 motif sequence situated in positions 93 to 99, the extended motif is composed of the canonical
217 motif and the neighboring residues which have a strong impact on binding from positions 85 to 99
218 (Figure 2b).

219

220 DHFR-PCA reports on the amount of protein complex formed, which depends on affinity and local
221 protein abundance. To differentiate between these two parameters, we measured the effect of
222 mutations on a Pbs2 interaction to a partner that does not depend on the SH3 binding motif. Hog1
223 binds Pbs2 distally to the SH3 binding motif and independently of Sho1 binding (Murakami *et al.*
224 2008) (Figure 1a). So, measuring Hog1-Pbs2 binding allows us to control for Pbs2 local
225 abundance. Pbs2 mutations that only affect Sho1 binding should not have a detectable effect in
226 the Hog1-Pbs2 DHFR-PCA, while Pbs2 mutations that affect Pbs2 stability or local abundance
227 will have an effect in the Sho1-Pbs2 as well as the Hog1-Pbs2 DHFR-PCA.

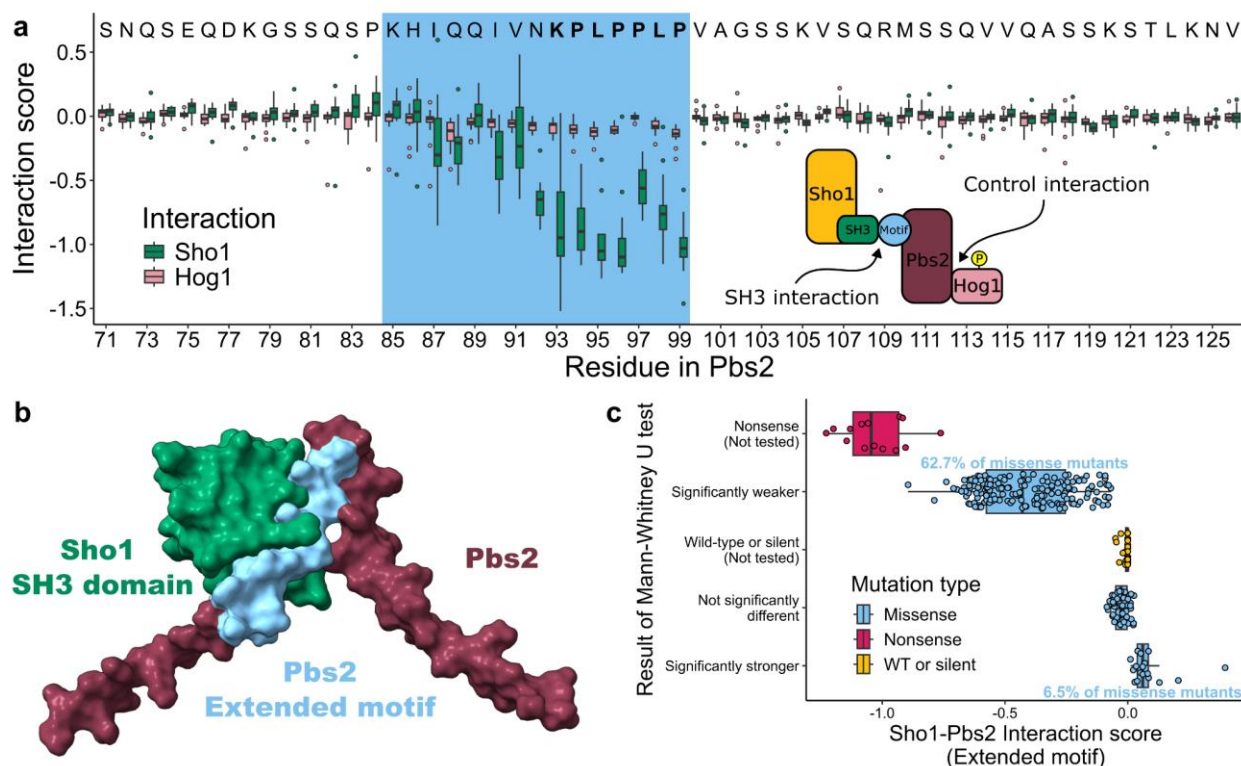
228

229 We found that most mutations in the surrounding region of the Pbs2 motif had little effect on Hog1
230 binding (Figure 2a). Furthermore, mutants that had a negative effect on Hog1-Pbs2 binding also
231 had a negative effect on Sho1-Pbs2 binding, suggesting that the reduction in signal results from
232 a loss of local abundance of Pbs2 (Figure S3). However, most mutations that affected Sho1
233 binding did not impact the Hog1 interaction, and therefore did not change the local abundance of
234 Pbs2. Strikingly, only mutations in the residues comprising the extended motif had Sho1-
235 interaction specific effects, while mutations outside the extended motif had either little effect or
236 destabilizing effects.

237

238

239



240

241 Figure 2. Mutations in Pbs2 within and around the binding motif affect binding to Sho1.
242 a) Effect of Pbs2 mutations in the surrounding region of the SH3 binding motif (interaction score,
243 normalized log2-fold change before and after selection using MTX), with either Sho1 or Hog1.

244 The wild-type residues of Pbs2 are indicated for each position at the top of the figure. The
245 positions comprising the extended motif are highlighted in blue, while the positions in the
246 canonical binding motif have the wild-type residue indicated in bold. Boxplots show the distribution
247 effects for each residue mutated to, and each residue is measured in between 3 and 18 replicates.
248 Nonsense mutants omitted. b) A predicted structure (AlphaFold2-Multimer) of the SH3 domain of
249 Sho1 (green) in complex with the Pbs2 region surrounding the motif (burgundy). The extended
250 motif in positions 85 to 99 is colored in light blue. c) Distribution of interaction scores between
251 Sho1 and Pbs2 single mutants in the extended motif DMS library (positions 85 to 100). Mutations
252 are colored and placed on the y-axis by the nature of the mutation, either a change to a stop
253 codon (nonsense), a change to the wild-type codon or a synonymous codon (WT or silent) or a
254 change to a codon coding for a different residue (missense). The missense mutants were
255 compared to the WT and silent mutations, using a Mann-Whitney U test with false discovery rate
256 correction. They were grouped into 3 categories: Significantly weaker ($p\text{-value} < 0.05$ and
257 negative interaction score), Not significantly different ($p\text{-value} > 0.05$) or Significantly stronger ($p\text{-value} < 0.05$ and positive interaction score).
258

259
260 Extended motif DMS library identifies mutations modulating interaction strength
261
262 In light of these results, we decided to focus solely on the extended motif of Pbs2, comprising
263 codons 85 to 99, and adding position 100 to verify no effects were taking place in the residue
264 immediately following the canonical motif. The DHFR-PCA on the initial DMS library of the entire
265 region surrounding the motif took place in a diploid strain. Consequently, a large part of Pbs2
266 binding occurred with the Sho1 copy which did not possess the DHFR F[1,2] fusion, and these
267 interactions did not contribute to the DHFR-PCA signal. Since this limited our ability to precisely
268 measure the Sho1-Pbs2 interaction, we built a new haploid strain containing both DHFR F[1,2]
269 on Sho1 and DHFR F[3] on Pbs2. We also constructed a Hog1-DHFR F[1,2]/Pbs2-DHFR F[3]
270 strain to once more measure the local abundance of Pbs2 mutants. These new strains capture
271 all Pbs2 binding to Sho1 or Hog1, therefore allowing for more sensitive measurements. We
272 inserted a second Pbs2 DMS library, comprising all possible single mutations in Pbs2 positions
273 85 to 100, into the two haploid DHFR strains, using the same CRISPR-Cas9 approach as the first
274 library. The interaction strength of the variants was measured using the DHFR-PCA as previously
275 (Figure S4, Figure S5). At this point, we filtered out the 12 mutants which had an interaction score
276 with Hog1 significantly different from wild type and synonymous Pbs2 mutants (Two-sided Mann-
277 Whitney U test with false discovery rate corrected $p\text{-value} < 0.05$) from our analysis (Figure S6).
278 As before, the goal was to disregard mutants which modulated the interaction through change of
279 local abundance or stability, which would affect both the Sho1 and Hog1 interaction.
280

281 The impacts on the Sho1-Pbs2 interaction were varied (Figure 2c, Figure S7, Table S2). Few
282 mutants had interaction scores as low as the nonsense mutants, suggesting that few single
283 mutations are able to completely prevent Sho1-Pbs2 binding. By comparing missense mutant
284 interaction scores to the wild type and synonymous mutants scores, we found that many missense
285 mutants had significantly stronger or weaker scores than the wild-type Pbs2 sequence (Two sided
286 Mann-Whitney U test with false discovery rate corrected $p\text{-value} < 0.05$). 18 mutants (6.5% of all
287 missense mutants) interacted significantly more strongly with Sho1 than wild-type Pbs2, while

288 173 mutants (62.7% of all missense mutants) interacted significantly more weakly than wild-type
289 Pbs2. The impact of mutants that reduced the interaction scores was generally greater.
290

291 As the Sho1-Pbs2 interaction is strengthened under osmotic stress (Maeda *et al.* 1995; Posas
292 and Saito 1997; Saito and Posas 2012), we also compared the interaction strength between these
293 two proteins in the presence and absence of 1 M of sorbitol (Figure S8). We found that interaction
294 scores in the presence and absence of sorbitol correlate strongly (Spearman's rho 0.98, p-value
295 < 2.2X10⁻¹⁶). The effects on binding were stronger in the presence of sorbitol, as a result of the
296 induction of the HOG signaling pathway. When sorbitol is present, strongly interacting Pbs2
297 mutants are even more often in contact with Sho1, increasing the number of reconstituted DHFR
298 complexes, while weakly interacting mutants are even further outcompeted by the strongly
299 interacting mutants. Still, the high correlation in interaction scores between these two conditions
300 indicates that Pbs2 mutants behave similarly in the presence and absence of osmotic stress, and
301 that the general strengthening or weakening effect of mutations does not depend on the activation
302 of the signaling pathway.
303

304 To validate the pooled measurements, we individually reconstructed 24 mutants spanning the
305 range of measured interaction scores in Pbs2-DHFR F[3] strains which were mated with the Sho1-
306 DHFR F[1,2] strain. We then measured the growth rate of these mated strains in growth assays
307 in DHFR-PCA medium. As with the competition assay, the growth rate is a proxy for interaction
308 strength, which reflects affinity in the absence of a change in abundance. The growth curve results
309 correlate strongly with the interaction scores (Spearman's rho 0.88, p-value 7.3x10⁻⁵ for
310 interactions in presence of 1 M sorbitol, spearman's rho of 0.73, p-value 2.9x10⁻⁶ for interactions
311 in absence of sorbitol), thus upholding the results of the competition assay (Figure S9a). To
312 validate further that the effects on interaction strength were not the result of noise or the result of
313 another source, we also performed a smaller scale competition assay DHFR-PCA, individually
314 reconstructing 67 mutants with varying interaction scores (Figure S10, Table S3). The
315 measurements of this validation assay correlated strongly with the assay on the DMS library of
316 the extended motif (Spearman's rho 0.98, p < 2.2X10⁻¹⁶ for interactions in presence of 1 M sorbitol,
317 spearman's rho of 0.98, p < 2.2X10⁻¹⁶ for interactions in absence of sorbitol), thus validating the
318 results of the measurement of the DMS library (Figure S9b). We also measured the effect of
319 mutations on cell proliferation by constructing strains with the same 67 mutations, but with no
320 DHFR tags. Cell growth and division should thus only depend on the effect of the mutations, and
321 not interaction strength. We undertook a pooled competitive growth assay in SC synthetic media
322 with 1 M of sorbitol, measuring how much each mutant proliferated. We found that all mutations
323 except nonsense mutations had no significant effect on cell proliferation (Welch's t-test false
324 discovery rate corrected p-value < 0.05) (Figure S11, Table S3). Interestingly, mutant I87W, which
325 is the strongest interacting mutant, seems to have a detectable, though not statistically significant,
326 deleterious effect on cell proliferation.
327
328
329
330
331

332

333 Structure prediction suggests a secondary contact between extended motif and Sho1

334

335 A crystal structure of the SH3 domain of Sho1 in complex with a 9 residue-long segment of Pbs2
336 reveals that the canonical motif occupies the entirety of the canonical binding pocket of Sho1
337 (Kursula *et al.* 2008). However, many mutations outside the canonical motif have a strong effect
338 on binding. These residues must affect the interaction of Pbs2 with Sho1, but it is unclear how.
339 One possibility is that certain residues in the extended motif are interacting with Sho1 outside of
340 the canonical binding pocket of the SH3 domain. This would not be unprecedented, as NMR
341 structures of different SH3 domains interacting with long peptides reveal interactions involving
342 residues outside of the canonical binding pocket, which affected the strength and specificity of
343 the interaction (Rickles *et al.* 1995; Feng *et al.* 1995; Stollar *et al.* 2009; Takaku *et al.* 2010; Gorelik
344 and Davidson 2012). No experimental structure has been determined for the entirety of Sho1 or
345 Pbs2, so we used structure predictions from AlphaFold-Multimer (Jumper *et al.* 2021; Evans *et*
346 *al.* 2022) to determine if binding outside the canonical binding pocket was likely to occur (Figure
347 S12). By modeling the entire Sho1 protein along with the surrounding region of the Pbs2 motif
348 (positions 71-126), we found potential interactions outside of the canonical binding pocket of
349 Sho1, mediated by residues neighboring the canonical binding motif of Pbs2 (Figure 3a). In the
350 structural model, a hydrophobic pocket is formed between the SH3 domain and a loop of Sho1,
351 which interacts with an alpha helix composed of Pbs2 positions 84 to 92 (Figure 3b). Interestingly,
352 all but one of the mutants in the extended motif which significantly increase interaction strength
353 are found in the positions comprising the helix. Certain Pbs2 residues towards the C-terminus
354 relative to the canonical motif are also predicted to be in proximity to Sho1, with 2 residues within
355 2 Å of Sho1, but as mutations in these positions did not have substantial effects on binding (Figure
356 2a), we decided to concentrate on residues in and near the extended motif.

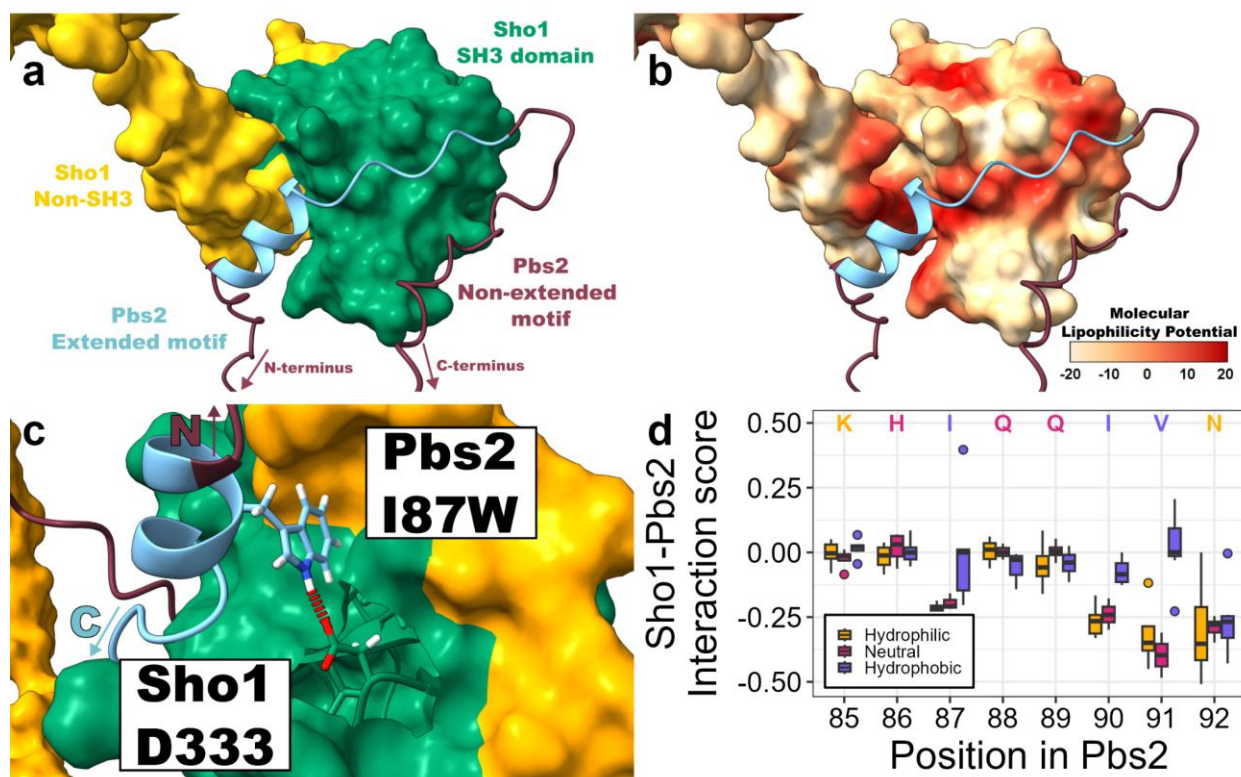
357

358 To help explain how different mutations could modify binding, we predicted the structures of the
359 5 Pbs2 variants possessing the strongest interaction strength with Sho1, using the same method
360 as with wild-type Pbs2 (Figure S12). In particular, I87W, which is the strongest interacting mutant
361 measured, positions its side-chain in close contact (1.77 Å) with the non-canonical hydrophobic
362 pocket, and particularly in a sub-pocket formed of both SH3 and non-SH3 residues. Additionally,
363 it is predicted to form a hydrogen bond with the aspartic acid side chain in position 333 of the
364 Sho1 sequence (Figure 3c). These two factors potentially explain its strong interaction strength
365 relative to all other Pbs2 variants. Of the other strengthening variants tested, H86W, V91L and
366 V91M all place a hydrophobic side chain in the non-canonical hydrophobic pocket, potentially
367 strengthening the interaction. For the last mutant tested, Q89D, the hydrophilic side-chain faces
368 away from the hydrophobic pocket, thus not disrupting the hydrophobic interaction, although it is
369 unclear how the interaction is strengthened (Figure S13).

370

371 We further reasoned that substituting a non-hydrophobic residue in one of the Pbs2 positions
372 which is predicted to contact the non-canonical hydrophobic pocket could interrupt this interaction,
373 and weaken the affinity. Indeed, when classifying the mutations in the alpha helix by their
374 hydrophobicity (Monera *et al.* 1995), we find that replacing the initially hydrophobic residues in
375 positions I87, I90, and V91 with a non-hydrophobic residue reduces the binding strength. In

376 general, a mutation to another hydrophobic residue in these positions has a weaker negative
377 impact on binding, and in the case of V91, many hydrophobic substitutions increase the
378 interaction strength (Figure 3d). Based on the results of the hydrophobic or non-hydrophobic
379 substitutions, we reasoned that these three positions situate their side chains in the non-canonical
380 hydrophobic binding pocket. This finding helps explain the strong interactions strength of Pbs2
381 mutant I87W, by showing the important role of hydrophobic interactions in position 87. The
382 predicted models of interactions between Sho1 and different Pbs2 variants, along with our
383 interaction score measurements suggest that residues outside the canonical binding motif of Pbs2
384 can interact directly with Sho1, and thus they have the capacity to modulate affinity.
385
386
387
388
389



390
391 Figure 3. Contacts mediated by positions outside the canonical binding motif of Pbs2 could
392 modulate binding

393 a) Structure of Sho1 in complex with residues 71 to 126 of Pbs2 as predicted by AlphaFold2-
394 Multimer (Jumper *et al.* 2021; Evans *et al.* 2022). The structure is positioned to show the helix on
395 Pbs2 interacting with a hydrophobic pocket on Sho1, while the canonical motif interacts with the
396 canonical binding pocket. The structure is colored by the different regions of Sho1 and Pbs2, as
397 indicated on the panel. The orientation of Pbs2 is shown by annotations indicating which end is
398 nearer the N-terminus and which end is nearer the C-terminus. b) Hydrophobicity map of the
399 predicted structure of Sho1, with high molecular lipophilicity potential (MLP) indicating a
400 hydrophobic surface, and low MLP indicating a hydrophilic surface. MLP calculated using

401 Chimera X 1.8. Positioning of both proteins, and coloring of Pbs2 as in panel a). c) Close-up of
402 the predicted structure of Sho1 with residues 71 to 126 of Pbs2 with mutation I87W. The side-
403 chain of W87 is shown, and a hydrogen bond (red dotted line) is predicted with D333 of Sho1.
404 Coloring of the proteins is as described in panel a). The orientation of Pbs2 is shown by
405 annotations indicating which end is nearer the N-terminus (N) and which end is nearer the C-
406 terminus (C). d) Boxplot of interaction scores of Pbs2 mutants for selected positions from the
407 DHFR-PCA of the DMS library of the extended motif, based on the hydrophobicity of the
408 substituted residue. The wild-type residue of Pbs2 for every position is indicated and colored
409 according to its hydrophobicity. Nonsense mutants omitted. Hydrophobicity for the different amino
410 acids was obtained from (Monera *et al.* 1995), and F, I, W, L, V, M, Y, C, and A were classified
411 as hydrophobic, T, H, E, S and Q were classified as neutral and R, K, N, G, P and D were classified
412 as hydrophilic.

413

414

415

416 Comparison of Sho1-Pbs2 binding to other SH3-motif pairs

417

418 As we propose a role in modulating interaction strength for the extended motif and the additional
419 binding pocket of Sho1, we wondered if these structures could play a part in modulating the
420 binding specificity of Pbs2 to Sho1. If this additional pocket were a unique structure among yeast
421 SH3 domains, that could increase the specificity of binding, as the Pbs2 extended motif could be
422 uniquely tuned to bind this unique feature. First, we generated a multiple sequence alignment of
423 yeast SH3 domain sequences with 25 adjacent residues on each side, to verify the conservation
424 of the amino acids forming the additional binding pocket. This window includes all residues
425 predicted to be in proximity to Pbs2 in Sho1. Apart from a few key residues in the SH3 domain,
426 we found no significant conservation of the positions which in Sho1 are predicted to be in proximity
427 ($< 5 \text{ \AA}$) to Pbs2 positions situated in the extended motif, but outside of the canonical motif (Figure
428 S14a). We reasoned that the structure of the additional binding pocket might be conserved, even
429 if the particular residues were not, so we used the MUSTANG (Konagurthu *et al.* 2006) tool to
430 carry out a multiple structural alignment on structure predictions of yeast SH3 domains with 25
431 neighboring residues, obtained from the AlphaFold Protein Structure Database (Varadi *et al.*
432 2022). We found that only the positions in the SH3 domains were structurally conserved, with no
433 significant structural conservation for the positions outside the SH3 domains (Figure S14b),
434 including those forming the additional binding pocket. We therefore conclude that the additional
435 binding pocket on Sho1 is a unique structural feature.

436

437 Even without a conserved structure of non-SH3 sequences, there are reports of three other yeast
438 SH3 domains binding extended motifs: Abp1, the second SH3 domain of Bem1 (referred to as
439 Bem1-2) and Nbp2 (Stollar *et al.* 2009; Takaku *et al.* 2010; Gorelik and Davidson 2012). We
440 tested whether there was an *in vivo* interaction between these SH3 domains tuned to bind
441 extended motifs, and the extended motif of Pbs2. To do so, we once again used a DHFR-PCA
442 assay, though this time measuring colony growth on solid medium as is routinely done for this
443 (Tarassov *et al.* 2008), with the SH3-containing proteins tagged with DHFR F[1,2] and Pbs2
444 tagged with DHFR F[3]. We used two variants of Pbs2: a wild-type, and a control where the

445 extended motif and the region surrounding it (positions 71 to 126, the same region covered in the
446 initial DMS library) were replaced by a neutral, flexible stuffer sequence.

447

448

449 We found that Abp1 and Nbp2 interact with Pbs2 with approximately the same strength as Sho1
450 does, while Bem1-2 does not detectably interact with Pbs2 (Figure 4a). However, Abp1 and Nbp2
451 also interact with the stuffed Pbs2 variant at the same level as the wild-type variant, indicating
452 that the interaction is not mediated by the Sho1-binding motif. Nbp2 is known to bind a second,
453 distal motif on Pbs2 through its SH3 domain (Mapes and Ota 2004), while Abp1 must bind Pbs2
454 through an unknown mechanism involving a different site than the one bound by Sho1. We
455 additionally measured the interaction with all other known yeast SH3-containing proteins, and
456 found that apart from Abp1 and Nbp2, all proteins interacted significantly less strongly with either
457 Pbs2 variant than Sho1 with wild-type Pbs2 (One sided Mann-Whitney U test with false discovery
458 rate corrected p-value < 0.05) (Figure S15). Additionally, measuring the interaction of Pbs2 with
459 a Sho1 variant where the SH3 domain was replaced by the neutral, flexible stuffer sequence
460 showed an interaction strength above the level of stuffed Pbs2 with the same Sho1 variant,
461 confirming the role of the non-SH3 portion of Sho1 in binding the extended motif of Pbs2 (Figure
462 S15, Sho1_stuffed). Together, these findings show that the extended motif of Pbs2 specifically
463 binds to Sho1 both inside and outside the SH3 domain, and doesn't interact with other SH3-
464 containing proteins *in vivo*.

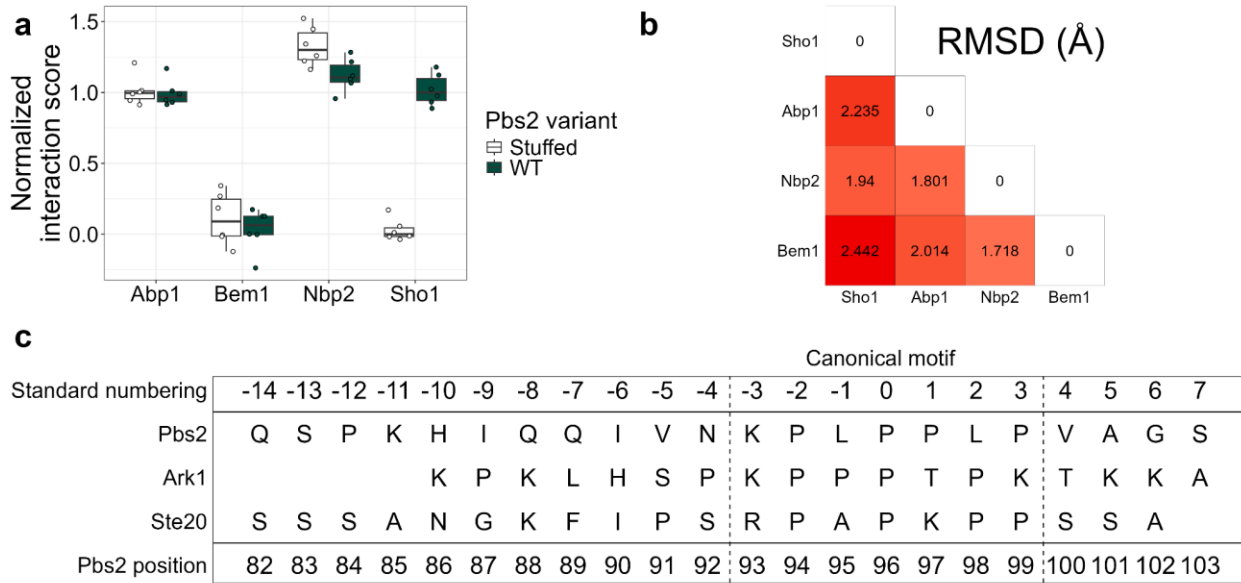
465

466 To determine whether we could explain the specificity of Pbs2 binding, we compared the predicted
467 structure of the Sho1-Pbs2 interaction to NMR structures of the Abp1-Ark1, Bem1-2-Ste20, and
468 Nbp2-Ste20 interactions, all of which include long peptides with lengths comparable to the
469 extended motif of Pbs2. The structures of the four SH3 domains and peptides are very similar,
470 with all peptides binding in the canonical binding pocket of their respective SH3 domains, and
471 extending towards the space corresponding to what we identified as the additional binding pocket
472 on Sho1 (Figure 4b, Figure S16). However, Abp1 and Nbp2 only bind the extended motif through
473 the SH3 surface, while Bem1-2 has a second, non-SH3 interface that forms a pocket with the
474 SH3 domain into which the extended motif fits, much like Sho1. However, this surface has no
475 structural or sequence similarity with Sho1 and has been previously identified as the Cdc42
476 interacting (CI) region (Takaku *et al.* 2010). Contrary to Sho1, this additional binding region is
477 located C-terminal to the SH3 domain.

478

479 There is little sequence conservation between the extended motifs of Pbs2, Ark1, and Ste20,
480 apart from the conserved positions of the canonical motifs. These extended motifs can be aligned
481 using a previously developed standard numbering, where the first conserved proline is designated
482 0, residues preceding the motif are numbered with decreasing negative numbers, and residues
483 following the motif are numbered with increasing numbers (Lim *et al.* 1994) (Figure 4c). The
484 binding specificity exhibited by Pbs2 may depend on the possible contacts with the different SH3
485 domains, and the non-SH3 surfaces in the cases of Sho1 and Bem1-2. Examining the different
486 motifs and their contacts with their respective interaction partners, we can compare Pbs2 to the
487 two other extended motifs, and in particular the positions which are in the extended motif but
488 outside the canonical binding motif, to establish determinants of specificity.

489
490 Foremost, Pbs2 binds using residues more distal from the canonical motif than either Ste20 or
491 Ark1. Contacts are predicted for Q(-14) as well as H(-10) on the predicted Sho1-Pbs2 structure,
492 which is not the case for any other interaction. In Pbs2, I(-9), which can have a large impact on
493 binding when mutated, contacts the hydrophobic residues L290 and Y293 on the non-SH3 surface
494 of Sho1. The equivalent position on Ste20, G(-9) contacts the polar residues Q240 and K243 in
495 the non-SH3 surface of Bem1, which would be unfavorable for the isoleucine in Pbs2. In Ark1
496 binding to Abp1, the residue at position (-9) contacts the SH3 domain (Figure 5a).
497
498 Position (-7) is important for binding in both Ste20 (F(-7)) and Ark1(L(-7)). When binding to their
499 respective partners, including both Bem1-2 and Nbp2 for Ste20, mutation of position (-7) to an
500 alanine reduced the strength of binding by at least an order of magnitude. Sequentially mutating
501 all positions in the extended motif to an alanine showed that position (-7) had the most impact of
502 any position outside the canonical motif in all cases (Stollar *et al.* 2009; Gorelik and Davidson
503 2012). In Pbs2, position (-7) is occupied by a polar glutamine, as opposed to the hydrophobic
504 residues found in the same position in the other two peptides. Also, in the predicted Sho1-Pbs2
505 structure, the side chain of Q(-7) is pointed away from Sho1 and is not predicted to have any
506 contacts, while in the other structures, the equivalent side chains are pointed towards the SH3
507 domains (Figure S17a).
508
509 Position (-6) also marks a difference, specifically between Pbs2 and Ark1. In Pbs2, I(-6) contacts
510 Y42 on the SH3 domain. In Ark1, H(-6) forms a salt bridge with an aspartic acid situated on a
511 different loop of the Abp1 SH3 domain (Figure 5b). The structural alignment of SH3 domains
512 indicates that Sho1 has a gap at the position of the salt bridge forming aspartic acid (Figure S14b,
513 position 112). The last major difference is in position (-4), where the residues in both Ste20 and
514 Ark1 make contact with an SH3 domain, while N(-4) in Pbs2 is not predicted to have any contacts.
515 As with position (-7), the polar side-chain is pointed away from the SH3 domain (Figure S17b).
516
517 Overall, we can see that the Pbs2 extended motif is very different from the other extended motifs
518 known to bind SH3 domains in yeast. The additional contacts in positions (-14) and (-10), the
519 differing contacts in positions (-9) and (-6), and the missing contact in position (-4) and especially
520 the important missing contact in position (-7) may preclude Pbs2 from binding to SH3 domains
521 other than Sho1. If this is truly the case, the presence of a non-conserved portion in the extended
522 motif allows much more differentiation in binding than solely the canonical motif.
523

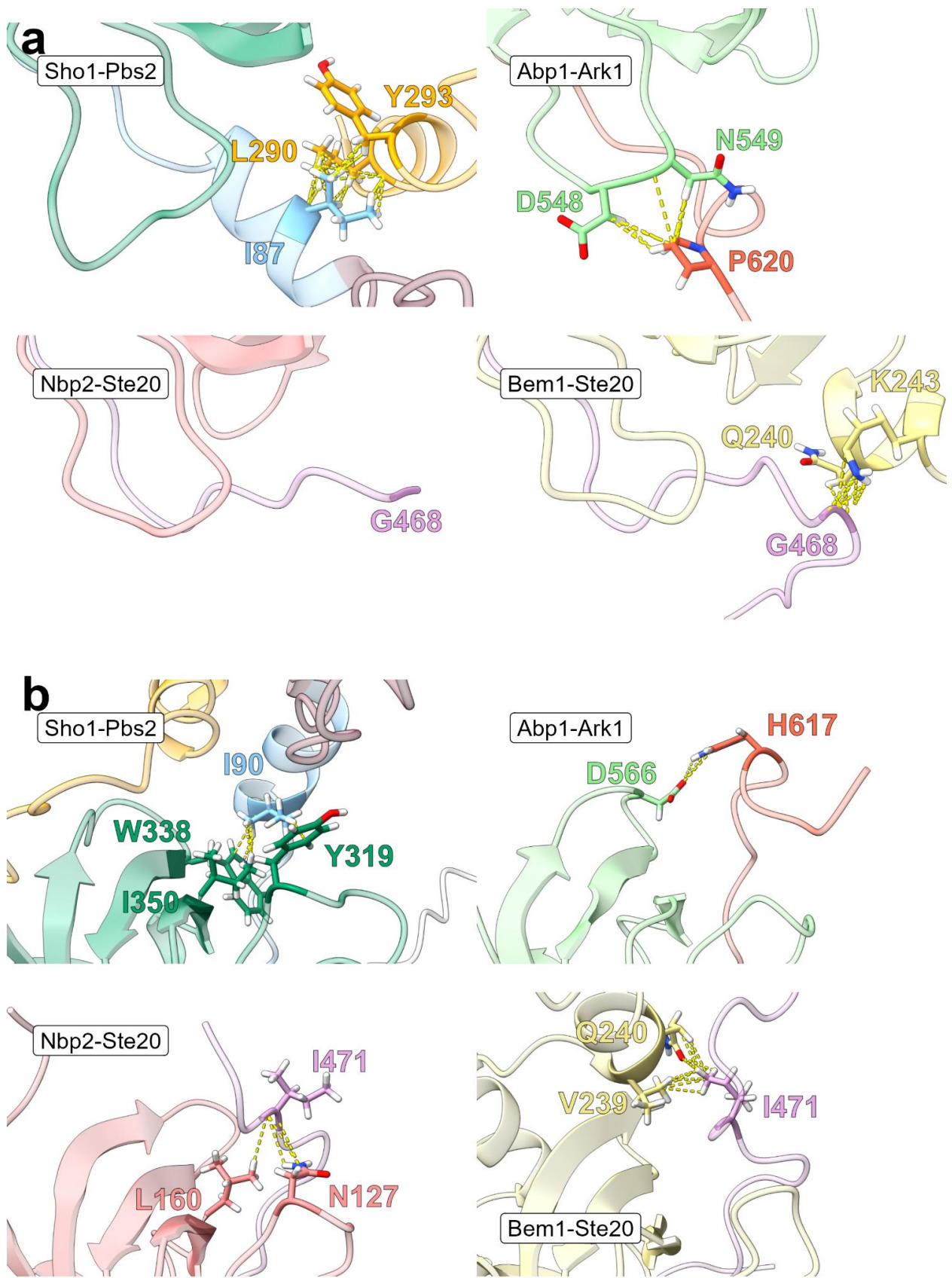


524

525

526 Figure 4. The Pbs2 motif binds specifically to Sho1, despite similarities of other SH3 domains and
motifs

528 a) Interaction score of wild-type Pbs2 (green) or Pbs2 where positions 76 to 126 have been
529 replaced with a flexible stuffer sequence (Stuffed, white) with select yeast SH3-containing
530 proteins. All replicates shown. Scores were normalized, with 1 being the median of Sho1 - wild-
531 type Pbs2 interactions and 0 being the median of Sho1 - stuffed Pbs2 interactions. b) Root mean
532 square deviation of atom locations between matching backbone atoms in each pair of structures,
533 as calculated using the R package bio3d (Grant *et al.* 2006). c) Sequences of Ste20, Ark1 and
534 Pbs2, with standard numbering according to the motif, to compare equivalent positions (Lim *et al.*
535 1994). For Ste20 and Ark1, the positions included are those present in the structures in panel b,
536 with Pbs2 positions chosen to overlap all represented positions.



538 Figure 5. Differing contacts between SH3-extended motif pairs

539 a) Visualization of the side-chains and contacts of position (-9) in the Sho1-Pbs2 predicted
540 structure, Abp1-Ark1 structure (PDB accession 2RPN), Nbp2-Ste20 structure (PDB accession
541 2LCS) and Bem1-2-Ste20 (PDB accession 2RQW). Sho1-Pbs2 predicted structure colored as in
542 figure 3a, with the SH3 domain of Sho1 in green, the non-SH3 portions of Sho1 in orange, the
543 Pbs2 extended motif in light blue and the rest of Pbs2 in burgundy. All four structures were
544 superimposed using the Chimera X tool “Matchmaker” (Pettersen *et al.* 2021) to minimize root
545 mean square deviance of backbone atom distances of the SH3 domains with Sho1, then pictures
546 were captured separately. Position (-9) and its contacts are kept opaque while the rest of the
547 structures are semi-transparent. b) Visualization of the side-chains and contacts of position (-6)
548 of the same structures as in panel a). All four structures were superimposed using the Chimera X
549 tool “Matchmaker” (Pettersen *et al.* 2021) to minimize root mean square deviance of backbone
550 atom distances of the SH3 domains with Sho1, then pictures were captured separately. Position
551 (-6) and its contacts are kept opaque while the rest of the structures are semi-transparent.
552
553
554
555
556
557
558
559
560

561 Discussion

562
563 Binding motifs face the double challenge of binding their partner with appropriate strength while
564 avoiding spurious interactions with non-partner proteins. Using deep mutational scanning libraries
565 of the Pbs2 binding motif and its surrounding sequences, we measured the impact of single
566 residue mutations on interaction strength with Sho1. We also predicted the structure of the Sho1-
567 Pbs2 interaction, and compared it to known structures of SH3-mediated interactions. We use
568 these comparisons to propose a number of ways in which the Pbs2 extended motif may bind
569 specifically to Sho1, and not other SH3 domains.
570

571 One important consideration in domain-peptide interactions is the potential trade-off between
572 interaction affinity and specificity. Previous studies on SH2 and PDZ domains, both domains that
573 bind short motifs similarly to SH3 domains, have put forth that mutants which bind with higher
574 affinity also possess lower specificity (Ernst *et al.* 2010; Haslam and Shields 2012; Kaneko *et al.*
575 2012; Karlsson *et al.* 2016), suggesting that high affinity and high specificity may be incompatible.
576 This represents an intuitive idea: a protein capable of having strong interactions with a certain
577 motif will also have more frequent and stronger spurious interactions with motifs of the same
578 family, which are physically and chemically similar. On the other hand, a computational assay
579 studying binding motifs, including SH3 binding motifs, found that an increase in affinity can lead

580 to an increase in specificity (Kelil *et al.* 2016). Other works have emphasized the importance of
581 the residues surrounding the canonical binding motif — in this case defined as K/RXXPXXP,
582 corresponding to positions 93 to 99 of Pbs2 — in determining both affinity and specificity (Li 2005;
583 Ivarsson and Jemth 2019). In fact, another study computed that nearly 30% of binding energy
584 from the binding motif was contributed by residues outside the canonical motif, and suggests that
585 the residues outside the canonical motif mostly play a role in determining specificity (Stein and
586 Aloy 2008). In our experimental work, we found that all mutations which significantly increase the
587 interaction strength between Sho1 and Pbs2 are situated outside of the canonical motif.
588 Consequently, the wild-type canonical motif could be already optimized for the strongest possible
589 interaction strength. This suggests different roles for the canonical motif and its neighboring
590 residues in determining affinity and specificity, with canonical motif residues optimized and
591 therefore more constrained, while the neighboring residues are less constrained and able to
592 increase affinity and specificity when mutated.

593

594 One interesting possibility that may explain the higher binding strength conferred by mutations to
595 certain residues outside the Pbs2 canonical binding motif is that the mutated residues may
596 interact with either residues outside the canonical binding pocket in the SH3 domain or even with
597 non-SH3 surfaces on Sho1. Non-binding pocket interactions have previously been observed in
598 multiple SH3-mediated interactions (Lee *et al.* 1996; Dalgarno *et al.* 1997; Li 2005; Stollar *et al.*
599 2009; Takaku *et al.* 2010; Gorelik and Davidson 2012; Gaussmann *et al.* 2024). Using predicted
600 protein complex structures generated by AlphaFold-Multimer, we were able to hypothesize that a
601 hydrophobic pocket is formed between the SH3 domain and a non-SH3 loop of Sho1, which
602 residues of the extended motif can fill. The presence of such a pocket can explain the increased
603 affinity of many Pbs2 mutants in the extended motif, as predicted structures of these models show
604 that substituted hydrophobic side chains can insert themselves into the predicted pocket. Perhaps
605 the disordered region encompassing the Sho1-binding motif can place itself in such a way to
606 maximize the hydrophobic interaction between any mutated side chain and the hydrophobic
607 pocket. These predicted structures may represent only one possible form of the Sho1-Pbs2
608 interaction, which may in reality be dynamic due to the disordered nature of the region surrounding
609 the Pbs2 motif. Nevertheless, they offer a potential example of binding mediated by positions
610 outside the canonical motif. By removing the need for affinity to be dependent only on canonical
611 binding motifs, the residues surrounding motifs could bind to protein surfaces which are less
612 conserved among SH3 domains, and thus easier to differentiate. The presence of unique
613 components, such as extended motifs or extended binding surfaces could therefore contribute to
614 specificity among domains of the same family. The hydrophobic pocket formed by both SH3 and
615 non-SH3 parts of Sho1 may represent an example of a unique structural feature which may help
616 differentiate Sho1 from other SH3 domains, and allow increased affinity to develop in Pbs2 without
617 increasing the affinity to other SH3 containing proteins. This proposed model of binding also
618 involves a larger number of residues in tuning affinity and specificity, potentially uncoupling affinity
619 and specificity and therefore avoiding a trade-off between these two phenotypes. Affinity and
620 specificity may only be linked for highly conserved residues and structures, such as the canonical
621 binding motif or the canonical SH3 binding pocket, but for less constrained residues, may develop
622 independently.

623

624 Studies on interaction domains have shown that SH3 domain mediated interactions are context
625 specific, meaning that the properties of the interactions depend not only on the domains
626 themselves, but also on the protein context. This context can be composed of many factors,
627 including the non-SH3 sequence of the protein, other proteins interacting with the SH3 containing
628 protein, and cellular localization (Dionne *et al.* 2022). SH3 mediated interactions therefore do not
629 simply depend on the SH3 sequence. For example, when inserting an SH3 domain into a different
630 protein or expressing an SH3 domain without its host protein, the SH3 domain's interaction profile
631 substantially changes (Dionne *et al.* 2021; Lemieux *et al.* 2024; Dibyachintan *et al.* 2024). Thus,
632 Pbs2 mutations may increase or decrease binding strength not only with the Sho1 SH3 domain,
633 but also within the Sho1 context. It is not entirely clear how Pbs2 mutations modulate binding
634 within the Sho1 context, but the binding of the Pbs2 extended motif to non-SH3 residues could
635 explain a large part of this phenomenon. Other causes could include stereochemical adjustments
636 of SH3 binding loops or changes which contribute to stabilizing or destabilizing interactions with
637 other Sho1 binding partners. There are observations of other proteins, namely Ste11 and Ste50,
638 interacting with the Sho1 SH3 domain outside of the canonical binding pocket (Zarrinpar *et al.*
639 2004; Tatebayashi *et al.* 2006). Changes to the Pbs2 peptide may affect the stability of the
640 interaction of these proteins, which are also involved in the osmotic stress response pathway.
641

642 Previous work has already focused on the binding of Pbs2 motif variants (Zarrinpar *et al.* 2003).
643 We replicate some of the findings of this previous work, for example, showing that mutations near
644 the canonical Pbs2 motif can cause both gain and loss of binding strength. This study also finds
645 that a promiscuous double mutant of the Pbs2 motif has lower fitness (Zarrinpar *et al.* 2003). We
646 find that, apart from nonsense variants, no mutants confer a significant loss of fitness. However,
647 Pbs2 mutant I87W has a noticeable, though not statistically significant, negative effect on cell
648 fitness (Figure S11). I87W is also the mutant which most increases the interaction strength, which
649 may be a cause of the slightly reduced fitness. Mutations which increase affinity have been
650 suggested to have deleterious effects, by reducing the dynamicity of the pathway, and impeding
651 dissociation of the partners (Wang *et al.* 2018). For the Sho1-Pbs2 interaction, previous work has
652 found that a mutation in the Sho1 SH3 domain that increased affinity also led to a small reduction
653 in cell growth (Marles *et al.* 2004), indicating that the wild-type affinity may be already optimized,
654 and that stronger binding may disrupt signaling.
655

656 In conclusion, we show that mutations in positions neighboring the canonical binding motif of Pbs2
657 can both increase and decrease binding strength with Sho1. We propose a role for residues
658 outside the canonical Pbs2 binding motif in increasing binding affinity independently of binding in
659 the canonical SH3 binding pocket. We hypothesize that Sho1 is similar to certain other yeast SH3
660 domains which bind longer motifs through additional binding pockets (Stollar *et al.* 2009; Takaku
661 *et al.* 2010; Gorelik and Davidson 2012), and propose mechanisms through which an extended
662 binding motif could better differentiate binding to different SH3 domains. Going forward, studies
663 of SH3-motif binding should consider a wider range of residues, both on the SH3 domain and
664 surrounding the motif. Our work, along with previous work by other groups, suggests that *in vitro*
665 work using isolated domains and shortened peptides does not capture the full picture of domain-
666 motif interaction. By understanding and harnessing the potential of extended motif binding,

667 researchers may be better able to understand the impact of motifs in cell signaling and disease,
668 and better able to use motif binding in technical and medical applications.
669
670

671 Methods

672
673 Growth conditions
674 *Escherichia coli* cells were grown in 2YT medium (1% yeast extract, 1.6% tryptone, 0.2% glucose,
675 0.5% NaCl, and 2% agar for solid plates) with shaking at 37 °C for liquid cultures. When specified,
676 100 µg/mL of ampicillin (Amp, Bioshop Canada) were added as a selection agent.
677 *Saccharomyces cerevisiae* cells were grown in YPD medium (1% yeast extract, 2% tryptone, 2%
678 glucose, and 2% agar for solid plates), synthetic complete medium buffered to a pH of 6.0 (0.174%
679 yeast nitrogen base without amino acids, without ammonium sulfate, 2% glucose, 0.134% amino
680 acid dropout complete, 0.1% monosodium glutamate, with 1% succinic acid and 0.6% NaOH as
681 buffer) or PCA medium (0.67% yeast nitrogen base without amino acids and without ammonium
682 sulfate, 2% glucose, 10% liquid drop-out without adenine, methionine, and lysine, and 200 µg/ml
683 methotrexate (MTX, Bioshop Canada) diluted in dimethyl sulfoxide (DMSO, Bioshop Canada),
684 and 2.5% noble agar for solid plates), as specified. When specified, 200 µg/mL of G418 (Bioshop
685 Canada), 100 µg/mL of nourseothricin (Nat, Jena Bioscience) or 250 µg/mL of hygromycin B (Hyg,
686 Bioshop Canada) were used as selection agents. Also, when specified, 1 M of sorbitol (Bioshop
687 Canada) was added to either liquid or solid PCA medium. Yeast cultures were grown at 30 °C
688 with agitation at 250 rpm. See Table S4 for details of all growth media used.
689

690 Cloning
691 All plasmids were constructed by Gibson assembly. As template for the *PBS2* DMS library
692 construction (pUC19-Pbs2, see below), a pUC19 plasmid backbone was amplified (Addgene
693 #50005, primers 1F and 1R, all primers detailed in Table S5), then digested for 1 hour at 37 °C
694 using SacI (New England Biolabs). This linearized plasmid was used for Gibson assembly with
695 an insert composed of a 248 base pair region of *PBS2* amplified from genomic DNA, using primers
696 that add homology arms (Primers 2F and 2R). For the CRISPR-Cas9 based insertion of
697 sequences, the pCAS plasmid (Addgene #60847) was modified as previously described (Ryan *et*
698 *al.* 2016) to change the sgRNA to target either the Sho1 binding motif of Pbs2 (pCAS-Pbs2,
699 primers 3F and 3R), the SH3 domain of Sho1 (pCAS-Sho1, primers 4F and 4R), or the stuffer
700 sequence which was inserted into *PBS2* (pCAS-stuffer, primer 5F and 5R) (Dionne *et al.* 2021).
701 Proper plasmid construction was verified using Sanger sequencing (Primers 6F and 6R) (Messing
702 1983).
703
704

705 Strain construction

706
707 All strains used are summarized in Table S6. Yeast strains were constructed with either the F[1,2]
708 or the F[3] fragments of an engineered murine DHFR protein fused to the C-terminus of different

709 proteins, to measure protein interaction strength as previously described (Tarassov *et al.* 2008;
710 Michnick *et al.* 2016). The transformed sequence contains the DHFR F[1,2] fusion sequence as
711 well as a nourseothricin resistance cassette, or the DHFR F[3] fusion sequence with a hygromycin
712 B resistance cassette. This allows selection of the strains with DHFR fragment fusions. The DHFR
713 F[1,2] tagged strains were derived from MAT α strain BY4741 (*his3Δ leu2Δ met15Δ ura3Δ*), while
714 the DHFR F[3] strains were derived from MAT α strain BY4742 (*his3Δ leu2Δ lys2Δ ura3Δ*). The
715 Hog1-DHFR F[1,2] strain and the Pbs2-DHFR F[3] strain used in the paper were taken from the
716 Yeast Protein Interactome Collection (Horizon Discovery) (Tarassov *et al.* 2008). The Sho1-DHFR
717 F[1,2] strain additionally had a 1X FLAG tag at the end of the fragment construct, and its
718 construction was described in a previous publication (Dionne *et al.* 2021). Briefly, the DHFR
719 F[1,2], the Nat cassette, a flexible linker and the FLAG tag sequence were amplified from the
720 pAG25-DHFR F[1,2]-linker-FLAG plasmid (Dionne *et al.* 2021) using primers with homology arms
721 matching the regions either side of the *SHO1* termination codon. The cassette was transformed
722 into BY4741 cells and integrated by homologous recombination. Further deletions were done in
723 the DHFR F[1,2] tagged strains in order to knock out *PBS2*, using the *LEU2* cassette from pUG37
724 (Gueldener *et al.* 2002), through homologous recombination (Primers 7F and 7R). Proper deletion
725 was verified by PCR (Primers 8 to 11) and sequencing (Gueldener *et al.* 2002). After the mating
726 of the DHFR F[1,2] MAT α strains with the Pbs2-DHFR F[3] MAT α , only one copy of *PBS2* is
727 present. This prevents the additional wild-type allele from influencing the measurements of
728 interaction strength of the variants.
729

730 The Pbs2 mutants of interest for the DHFR-PCA growth curves were constructed from the Pbs2-
731 DHFR F[3] fusion strain. First, the region surrounding the Sho1 binding motif of Pbs2 (codons 71
732 to 126) was replaced with a stuffer sequence (GGCGGAAGTTCTGGAGGTGGTGGT) that
733 translates into a flexible linker sequence (GGSSGGGG), by co-transformation of the pCAS-Pbs2
734 plasmid, and of a repair template consisting of the stuffer sequence flanked by homology arms
735 matching the sequences around codons 71 to 126 of *PBS2* (produced by amplifying the stuffer
736 sequence with primers 12F and 12R), following a previously published protocol (Ryan *et al.* 2016).
737 This produced the Pbs2-stuffed-DHFR F[3] strain, which was used for the construction of the
738 individually reconstructed mutants, for the construction of the DMS libraries (see below), and also
739 as a control to measure Pbs2 binding to SH3-containing yeast proteins. The individually
740 reconstructed mutants contain all mutants used in a previous paper exploring Pbs2 mutants
741 (Zarrinpar *et al.* 2003), including a P94A+P97A double mutant. The mutants were individually
742 constructed by co-transforming the Pbs2-stuffed-DHFR F[3] strain with the pCAS-stuffer plasmid
743 targeting the aforementioned stuffer, and synthesized oligonucleotide sequences corresponding
744 to the desired mutation (Integrated DNA Technologies) (Table S7). The stuffed strain as well as
745 all reconstructed strains were verified by PCR and Sanger sequencing (Primers 13F and 13R).
746 The pCAS plasmids were purged by growth in liquid YPD without G418, and loss of the plasmid
747 was verified by lack of growth on YPD+G418 plates.
748

749 For the extended motif DMS library and the individually reconstructed mutants used in the
750 validation competition assays, three additional haploid strains were built, into which Pbs2 DHFR
751 mutations were inserted. The first two strains were Hog1-DHFR F[1,2]/Pbs2-stuffed-DHFR F[3]
752 and Sho1-DHFR F[1,2]/Pbs2-stuffed-DHFR F[3]. These were built by adding the DHFR F[1,2] tag

753 to either *HOG1* or *SHO1* in the MAT α Pbs2-stuffed-DHFR F[3] strain previously constructed. The
754 DHFR F[1,2] moieties were amplified from plasmid pAG25-DHFR F[1,2]-linker-FLAG plasmid
755 using primers with homology arms to either the *HOG1* or *SHO1* locus (Primers 14 F to 15R)
756 (Dionne *et al.* 2021). Proper tagging was verified using PCR and Sanger sequencing (Primers 16
757 to 18) (Freschi *et al.* 2013; Dionne *et al.* 2021). The third strain was Pbs2-stuffed, which was used
758 to measure the proliferation of mutants without the effect of the DHFR fragment. This was
759 constructed in the haploid strain BY4742, using the same strategy to insert the stuffer into *PBS2*
760 as detailed above.

761
762 The selected Pbs2 mutants for the validation assay were constructed in these three same strains
763 by transformation with repair templates containing the mutations of interest, formed through fusion
764 PCR. Briefly, forward and reverse primers were designed for each mutant to be constructed,
765 which contained the mutated sequence instead of the wild-type sequence (Primers 19F to 110R).
766 These primers were used for separate PCR amplification of the *PBS2* sequence along with either
767 common forward or reverse primers (Primers 111F and 111R), to create two overlapping
768 fragments. These were combined in a second PCR using only the two common primers, which
769 fused the overlapping sequences together, to create a single fragment of 338 base pairs, which
770 was identical to *PBS2* except for the mutated codon of interest. These fragments were
771 transformed into DHFR F[1,2]/Pbs2-stuffed-DHFR F[3] strains using the CRISPR-Cas9 strategy
772 described above. Mutants were confirmed by PCR and sequencing (Primers 112F and 112R).
773 Most mutations were constructed in all three DHFR strains, but a certain number could only be
774 built in one or two of the strains. The successfully constructed mutants are listed in Table S6.
775

776 For the DHFR-PCA screen on solid media, the previously constructed wild-type Pbs2-DHFR F[3]
777 and Pbs2-stuffed-DHFR F[3] were used. The SH3-containing proteins DHFR F[1,2] strains were
778 obtained from the Yeast Protein Interactome Collection (Horizon Discovery). A version of Sho1
779 was also built where the entire SH3 domain was replaced by the same flexible stuffer used in the
780 Pbs2-stuffed strain. As with Pbs2, the stuffer was amplified using primers adding homology to the
781 sequences either side of the Sho1 SH3 domain locus (Primers 113F and 113R). The stuffer was
782 inserted into the Sho1 sequence by cotransformation of the pCas-Sho1 plasmid and the repair
783 template of the stuffer with homology arms. Proper stuffing was verified by PCR and Sanger
784 sequencing (Primers 114F and 114R).

785
786 Construction of the surrounding region DMS library
787

788 The initial DMS library covering the surrounding region of Pbs2 was constructed as previously
789 reported (Dionne *et al.* 2021). 56 codons (168 nucleotides) were targeted, which correspond to
790 codons 71 to 126 of the YJL128C/PBS2 ORF.

791
792 A degenerate oligonucleotide was designed for each codon to be mutated, with the three
793 nucleotides of the mutated codon replaced by an NNN codon (Primers 115 to 170). This series of
794 56 oligonucleotides was used to amplify pUC19-Pbs2, in a two-step PCR procedure (Miyazaki
795 2011). At all steps, the different codons were kept in separate reactions and the mutants for each
796 codon were created in separate reactions. In the first amplification, a megaprimer was created

797 which includes the *PBS2* coding sequence using the degenerate oligonucleotide and a common
798 reverse primer (Primer 171R). The megaprimer thus carries the DMS library for one codon. In the
799 second PCR step, this megaprimer was used to amplify the entire plasmid. The PCR products
800 were digested with *DpnI* (New England Biolabs) at 37°C for 1 hour to remove the original
801 methylated template, and keep only the mutated plasmids amplified by the megaprimer. The
802 remaining mutated amplified but unligated plasmids were transformed into chemocompetent *E.*
803 *coli* cells strain MC1061, and plated on solid 2YT+Amp. The amplified plasmids were ligated and
804 thus recircularized in the cells. All transformations resulted in hundreds of colonies and these
805 colonies were suspended in 5 mL of 2YT. Their plasmids were extracted using a miniprep plasmid
806 extraction kit (Presto Mini Plasmid Kit, Geneaid) to obtain a plasmid library containing all the DMS
807 mutants. Prepared libraries were sequenced using 300-PE MiSeq technology (see DNA
808 sequencing section), to verify that the desired codon diversity was present. Once diversity was
809 confirmed, the libraries were amplified from the plasmids (Primers 172F and 172R), and
810 transformed into the Pbs2-stuffed-DHFR F[3] yeast strain using the CRISPR-Cas9 strategy
811 described in the strain construction section.
812

813 Transformed cells were plated on solid YPD+G418+Hyg for selection, and then resuspended in
814 liquid YPD. The optical density of each suspension (each codon) was measured and all
815 suspensions were pooled into a masterpool, with 5 optical density units (OD) added for each
816 codon. Frozen glycerol stocks were prepared for the individual suspensions of each codon, and
817 multiple stocks were prepared for the masterpool. Genomic DNA was extracted from the
818 masterpool using phenol/chloroform DNA extraction (Amberg *et al.* 2005), and as before, the
819 library was sequenced to verify diversity. At this point, three codons had unsatisfactory diversity.
820 A new template was created for codons 103 and 119 using fusion PCR, creating a sequence of
821 967 base pairs around the mutated codon, using the original degenerate primers as well as new
822 reverse degenerate primers to create an NNN codon at either codon 103 or 119 (Primers 173 to
823 175). For codon 88, a new template was ordered as an oligonucleotide of 503 base pairs (Twist
824 Bioscience), around codon 88, which is replaced by an NNN codon. These templates were
825 transformed into Pbs2-stuffed-DHFR F[3] as described above, and diversity at the desired codon
826 was verified with Sanger sequencing. The three supplementary cultures were pooled into the
827 masterpool, with an OD corresponding to 1/56th of the OD of the master pool.
828

829 DHFR-PCA competition assay for surrounding region DMS library

830
831 The PCA selection followed a previously published protocol (Dubé *et al.* 2022). Three liquid
832 cultures were started, each from 100 µL of the masterpool containing all mutated codon positions,
833 in SC complete medium. These cultures were incubated at 30 °C for 16 hours. 300 µL of this
834 preculture was mixed with 150 µL of either Sho1-DHFR F[1,2] or Hog1-DHFR F[1,2], and 1.2 mL
835 of fresh liquid YPD. These mixes of strains were left to mate for 8 hours at 30 °C with agitation.
836 The mated diploid cells were then selected in two successive cycles of diploid selection in liquid
837 YPD+Nat+Hyg at 30 °C with agitation. The first cycle consisted of a 5/12 dilution of the mating
838 culture in 3 mL of liquid YPD for 16 hours, and the second cycle consisted of a 1/10 dilution in 3
839 mL of liquid SC media for 24 hours. A volume equivalent to 5 OD was spun down and the
840 supernatant was removed, to form a cellular pellet, which was stored at -80 °C. This is the initial

841 time point used for sequencing. The selected diploid cultures were then diluted to 0.1 OD/mL in
842 15 mL of liquid PCA medium with either 200 µg/mL of methotrexate with 1 M of sorbitol, the same
843 concentration of methotrexate without sorbitol, or a control without methotrexate but with 1 M
844 sorbitol. This PCA selection was grown without light for 96 hours, except for the control cultures
845 which were saturated after 24 hours. After this first growth cycle, the cultures were diluted 0.1
846 OD/mL into 15 mL of fresh liquid PCA medium, and a 5 OD pellet was spun down and stored at -
847 80 °C. The second PCA cycle lasted the same amount of time, and at the end, as many 5 OD
848 pellets as possible were prepared from each culture. Genomic DNA was extracted from the pellets
849 of the second diploid selection cultures and the second PCA selection culture. The Pbs2 locus
850 was amplified and sequenced, as described in the DNA sequencing section.
851

852 Construction of the extended motif DMS library

853 A second DMS library was constructed of the extended motif of *PBS2*, comprising codons 85 to
854 100. An oligonucleotide pool (Integrated Data Technologies, Table S8) was synthesized
855 containing all possible NNK codons (K indicating either a G or T nucleotide) for the 16 codon
856 region of interest, with homology arms for a total length of 248 base pairs. This pool was integrated
857 into 2 different yeast strains: Sho1-DHFR F[1,2]/Pbs2-stuffed-DHFR F[3] and Hog1-DHFR
858 F[1,2]/Pbs2-stuffed-DHFR F[3], to allow respectively for PCA measurements of Sho1-Pbs2
859 interaction in a haploid strain, and PCA measurements of Hog1-Pbs2 interaction in a haploid
860 strain.
861

862 The mutant pool was integrated into these strains by replacing the Pbs2 stuffer using the CRISPR-
863 Cas9 strategy described in the strain construction section. As before, the integrated libraries were
864 sequenced to verify diversity. Transformed yeast libraries were stored at -80 °C.
865

866 DHFR-PCA competition assay for extended motif DMS library

867 The liquid PCA selection for the haploid double DHFR tagged strains was done following the
868 same protocol as the first DHFR-PCA selection, only ignoring the mating step. However, a fourth
869 control condition of PCA medium without methotrexate and without sorbitol was added. Three
870 replicate pools were done for each growth condition. Frozen pellets were prepared as in the first
871 DHFR-PCA selection.
873

874 Validation DHFR-PCA competition assay of individually reconstructed mutants

875 The individually reconstructed validation strains were pooled by combining 100 µL of saturated
876 overnight culture of each mutant in YPD. 6 pools were made for each condition, three pools each
877 from two individual reconstructed colonies of the mutant. The same conditions were used as the
878 second liquid PCA selection: PCA medium both with and without 1 M of sorbitol and with and
879 without methotrexate for the DHFR tagged strains. For the cell proliferation measurements, SC
880 medium with and without 1 M of sorbitol was used. Two cycles of selection were done, with 96-
882 hour cycles for the conditions with methotrexate and 24 hour cycles for the conditions without
883 methotrexate, and the SC medium. Frozen pellets were prepared as for the previous liquid PCA
884 selections.
885

885

886 DNA sequencing

887

888 DNA sequencing was done in generally the same manner for all experiments, with minor changes
889 in certain cases. DNA was extracted from the frozen pellets using a standard phenol/chloroform
890 genomic DNA extraction protocol (Amberg *et al.* 2005). The extracted DNA was amplified and
891 barcoded using a Row-Column DNA barcoding strategy as previously described (Dubé *et al.*
892 2022). From the extracted genomic DNA, the *PBS2* region of interest was amplified using primers
893 containing 3' overhangs which allow a second amplification to add barcodes (Primers 176F and
894 176R). PCR products were diluted 1/2500, and used as a template to add row and column
895 barcode primers onto the sequence, with a unique combination of 5' and 3' barcodes for each
896 replicate in each condition. The row-column barcode primers were previously described (Dubé *et*
897 *al.* 2022). PCR products were migrated on an agarose gel, and DNA concentrations were
898 estimated based on band size using the Image Lab software (BioRad Laboratories). Samples
899 were then pooled with different volumes to obtain the same quantity of DNA from each sample.
900 The pools were purified using magnetic beads, measured using a NanoDrop (ThermoFisher), and
901 diluted to 0.1 ng/µL. The diluted pools were then amplified with primers adding a second set of
902 barcodes, called plate barcodes (Dubé *et al.* 2022). These double-barcoded pools were purified
903 on magnetic beads, and sent for sequencing on Illumina NGS machines. Unique combinations of
904 barcodes were used to identify the DNA extracted from each pellet in each replicate of each
905 condition. The sequencing of the first DHFR-PCA, on the larger region surrounding the *Pbs2* motif
906 was done using Illumina NovaSeq paired-end 250 base pair technology (CHUL sequencing
907 platform, Quebec, Canada), while all other sequencing was done using Illumina MiSeq paired-
908 end 300 bp technology (IBIS Genomic Analysis Platform, Quebec, Canada).

909

910 After preliminary analysis of the sequencing of the DNA from the pellets of the DHFR-PCA on the
911 extended motif DMS library, it was determined that more reads would be needed. Additional
912 sequencing libraries were prepared fresh from the original DNA extractions. Instead of using a
913 row-column barcoding approach, the *PBS2* region was amplified using primers (Primers 177F
914 and 177R) with homology arms allowing the addition of Illumina Nextera barcodes (Illumina).
915 These allow automated demultiplexing by the Illumina MiSeq instrument. All other steps were as
916 described above.

917

918

919 Analysis of DNA sequencing results

920 The variant frequency in DMS libraries during construction and in the DHFR-PCA and proliferation
921 screens was evaluated using custom scripts based on already published work (Després *et al.*
922 2022). Python libraries pandas 1.5.2 (The pandas development team 2023), matplotlib 3.6.2
923 (Hunter 2007) and numpy 1.24.1 (Harris *et al.* 2020) were used for data manipulation and
924 visualization. Quality was assessed using FastQC 0.12.1 (Andrews 2010). Reads were trimmed
925 using Trimmomatic 0.39 (Bolger *et al.* 2014), then demultiplexed using bowtie 1.3.1 for the
926 sequencing of the surrounding region DMS library (Langmead *et al.* 2009), Interstellar 1.0
927 following the RCP-PCR configuration for the first sequencing run of the extended motif DMS
928 library (Kijima *et al.* 2023) and cutadapt 4.7 for the validation competition assay sequencing

929 (Martin 2011). The second sequencing run for the extended motif DMS library was barcoded using
930 Illumina Nextera primers, and was thus automatically demultiplexed by the sequencing
931 instrument. Forward and reverse reads were then merged using the PANDAseq software (Masella
932 *et al.* 2012). Next, identical reads were grouped using vsearch (Rognes *et al.* 2016), and aligned
933 to the wild-type *PBS2* sequence using the needle function from the EMBOSS software (Rice *et*
934 *al.* 2000). From this, the frequency of each variant was obtained.
935
936

937 From the frequency of each variant, the interaction scores and selection coefficients of each
938 variant were calculated using custom R 4.3.1 (R Core Team 2023) scripts. The R package
939 collection tidyverse (Wickham *et al.* 2019), as well as the packages rstatix 0.7.0 (Kassambara
940 2021), ggpubr 0.4.0 (Kassambara 2020) and bioseq 0.1.4 (Keck 2020) were used for data
941 analysis. R packages ggExtra 0.10.1 (Attali and Baker 2023), ggrepel 0.9.4 (Slowikowski 2023),
942 GGally 2.2.0 (Schloerke *et al.* 2023) and cowplot 1.1.1 (Wilke 2020) were used for data
943 visualization. Briefly, variant counts were imported, identified by the mutation type (wild type,
944 nonsense, missense or silent) then transformed into frequencies by dividing each variant count
945 by the total number of counts present in that sequencing library. The interaction score was
946 calculated as the log-2-fold-change of the frequency of each variant at the end of the second cycle
947 of methotrexate selection and the frequency of each variant after the selection for diploids (so
948 immediately preceding the methotrexate selection). These log-2-fold-change scores were
949 rescaled for each library, so that the median of nonsense codons was equivalent to -1 and the
950 value of wild-type variants was 0. Variants were then filtered to keep only those that had 20 or
951 more reads detected after diploid selection, in order to remove bias caused by low read counts
952 leading to inflated scores. Next, a unique score was calculated for each variant by taking the
953 median score of all codons coding for the same amino acid variant in all replicates of the same
954 condition. Scores were only kept for amino acid variants that had at least 3 replicates from any
955 combination of codons not filtered out. For the competition assay of cell proliferation, the number
956 of generations elapsed during the selection for each replicate was calculated, as the log-2-fold-
957 change the optical density of the cultures at the end and at the beginning of the growth cycles.
958 The selection coefficient for each variant was calculated as follows:
959

$$960 s = \frac{\ln\left(\frac{\text{variant frequency after PCA selection}}{\text{variant frequency before PCA selection}}\right) - \ln\left(\frac{\text{wt frequency after PCA selection}}{\text{wt frequency before PCA selection}}\right)}{\text{number of generations}}$$

961
962 The frequency of the wild type used is the frequency of the wild type in the same replicate as the
963 variant. The same filtering criteria were used for the proliferation assay as for the DHFR-PCA.
964

965 When measuring the interaction scores of the preliminary and extended motif DMS libraries, we
966 also included control conditions without methotrexate, the selective agent allowing measurement
967 of DHFR fragment reconstitution. The measurements in this condition should not give any
968 information about interactions between *Pbs2* and *Sho1*, but can inform us about any other defects
969 in the mutant strains. We calculated DMSO scores for growth in the control condition in the same
970 way as the interaction scores. We noticed that some nonsense mutants had growth scores

971 comparable to wild-type Pbs2, and that some silent mutants had growth scores comparable to
972 nonsense mutants. These abnormal scores could indicate defects in the strains, possibly resulting
973 from the Cas9 mediated mutation process. We statistically verified which nonsense and silent
974 mutants were abnormal by comparing every nonsense or silent mutation to all other nonsense or
975 silent mutations (Two-sided Mann-Whitney U test, $p < 0.05$). The mutants which were significantly
976 different were removed from the interaction score dataset. Similarly, we wanted to verify that no
977 missense mutants had any defects caused by other sources than the interaction. We statistically
978 verified which mutants had defects in the control condition by comparing each missense mutant
979 to the nonsense mutants (Two-sided Mann-Whitney U test with false discovery rate corrected p-
980 value > 0.05). The missense mutants which were not significantly different from the nonsense
981 mutants were also removed from the interaction score dataset.
982

983 We also removed from the interaction score dataset the mutants for which an abundance change
984 was detected through gain or loss of interaction strength between Pbs2 and Hog1, as explained
985 in the results section. Pbs2 missense mutants that had an interaction strength with Hog1 which
986 was significantly different from wild-type Pbs2 and silent mutations (Two-sided Mann-Whitney U
987 test with false discovery rate corrected p-value < 0.05), either in the presence or absence of
988 sorbitol, were removed from the datasets.
989

990

991 DHFR-PCA growth curves of individually reconstructed mutants

992

993 Growth curves were measured for individually reconstructed Pbs2 mutants in DHFR-PCA
994 medium, to validate Pbs2 interaction strength measurements. The DHFR F[3] tagged strains with
995 the mutations were mated with a Sho1-DHFR F[1,2]/*pbs2::LEU2* strain, in order to produce
996 diploids with complementary DHFR fusions. To mate these strains, 50 μ L of precultures of each
997 strain were mixed into 900 μ L of YPD and incubated at 30 °C overnight without agitation. 2 μ L of
998 each mated culture was spotted on solid YPD+Nat+Hyg, to select for diploids. Exponential phase
999 precultures of diploids were diluted to 0.1 OD/mL in 80 μ L of PCA medium, in a 384 well plate, in
1000 4 replicates, at 30 °C. Cultures were grown either with and without 200 μ g/mL of methotrexate,
1001 and with and without 1 M sorbitol. The optical density of each well was measured every 15 minutes
1002 in a Tecan Spark plate reader (Tecan). Growth curves were analyzed using a custom script written
1003 in R (R Core Team 2023), using the tidyverse package collection (Wickham *et al.* 2019) and the
1004 R package ggpubr 0.6.0 (Kassambara 2020). A function was written to find the maximal
1005 instantaneous growth rate for each well. Mutant P94R was disregarded, as growth of all replicates
1006 in the control condition in the absence of methotrexate was much lower than all other samples,
1007 suggesting a problem with strain construction.
1008

1009

1010 Structure prediction

1011

1012 Structure predictions were done for Pbs2 mutants in complex with Sho1 using AlphaFold 2.3.2
1013 and the AlphaFold-Multimer implementation (Jumper *et al.* 2021; Evans *et al.* 2022). Default
1014 options were used, and only the top scoring model for each mutant was relaxed. For Sho1, the

1015 sequence of the entire protein was used for prediction (Uniprot entry P40073). For Pbs2, residues
1016 71 to 126 were used for the prediction (Uniprot entry P08018). Predicted structures were
1017 visualized using ChimeraX 1.8 (Pettersen *et al.* 2021).

1018

1019 Sequence and structural alignments

1020 The protein sequences of 24 yeast SH3-containing sequences were obtained from the
1021 alliancemine server (Bult and Sternberg 2023). The sequence of the SH3 domains plus 25
1022 residues on each side was extracted from the complete protein sequences using the SH3 location
1023 information from Interpro (Paysan-Lafosse *et al.* 2023), and a custom R script. When an SH3
1024 domain was within less than 25 residues of the N- or C-terminus of a protein, the sequence up to
1025 the terminus was used. The sequences of these SH3 domains and adjoining regions were aligned
1026 using mafft 7.526, using the L-INS_i (local alignment) algorithm with the command line :
1027 "/usr/bin/mafft" --localpair --maxiterate 16 --inputorder "<input_file>" > "<output_file>" (Katoh and
1028 Standley 2013). For the structural alignment, we used previously predicted structures from the
1029 AlphaFold Protein Structure Database (Varadi *et al.* 2022). Using the R packages
1030 AlphaMissenseR (Morgan and Nguyen) and bio3d (Grant *et al.* 2006), we downloaded the
1031 predicted structures of the 24 same yeast SH3-containing proteins from the AlphaFold Protein
1032 Structure Database, and trimmed the pdb files to only contains residues composing the SH3
1033 domains as well as 25 residues on each side of the domain. To align the predicted sequences,
1034 we used the MUSTANG 3.2.4 tool, with the command line ./bin/mustang-3.2.3 -f ./path_to_files.txt
1035 -F fasta -o SH3_flanking -s off (Konagurthu *et al.* 2006). The ./path_to_files.txt file contains the
1036 paths of all trimmed pdb files.

1037

1038 DHFR-PCA on solid media against SH3 domain-containing proteins

1039

1040 The DHFR-PCA on solid media was based on previous work (Tarassov *et al.* 2008; Rochette *et*
1041 *al.* 2015). All colony manipulation was done using a robotic pin tool platform (BM5-SC1, S&P
1042 Robotics Inc.). The strains containing DHFR F[1,2]-tagged SH3-containing proteins and Pbs2-
1043 DHFR F[3] were taken from the Yeast Protein Interactome Collection (Horizon Discovery). The
1044 Pbs2-stuffed-DHFR F[3] strain is the same used for DMS library construction, and is described in
1045 the strain construction section. Cultures were started from frozen stocks in YPD with
1046 nourseothricin for DHFR F[1,2] strains and hygromycin B for DHFR F[3] strains, in deep welled
1047 96-well plates.

1048

1049 Colonies were cherry picked from the 96-well plates, and arrayed onto YPD+Nat plates for the
1050 DHFR F[1,2] strains or YPD+Hyg plates for the DHFR F[3] strains, in a 384 colony array. The
1051 DHFR F[1,2] strains were organized into a randomized pattern to avoid any effects caused by
1052 neighboring colonies. Each 384 colony plate of DHFR F[3] strains contained only copies of the
1053 same variant. The 384 colony arrays were condensed into 1536 colony arrays on YPD+Nat or
1054 YPD+Hyg, with the randomized DHFR F[1,2] pattern repeated four times. The outer two rows and
1055 columns of the 1536 arrays were composed of LSM8-DHFR F[1,2] and CDC39-DHFR F[3], which
1056 grow well on PCA medium and serve to avoid any measurement bias from being on the edge of
1057 the array for the interactions of interest. The 1536 colony arrays were mated together by pinning
1058 the repeated DHFR F[1,2] array onto YPD plates, and then pinning one of the DHFR F[3] arrays

1059 onto each plate. In this collection of arrays, each interaction between an SH3 containing protein
1060 and a Pbs2 variant was measured in 5 or 6 replicates. After 48 hours of mating at 30 °C, the
1061 mated colonies were pinned onto YPD+Nat+Hyg plates to select for diploid cells. Two growth
1062 cycles of 48 hours at 30 °C on YPD+Nat+Hyg were done. After diploid selection, the plates were
1063 photographed using an EOS Rebel T5i camera (Canon), to verify that all colonies grew correctly.
1064 The mated arrays were then pinned onto solid PCA medium plates, either with or without
1065 methotrexate, and with 1 M of sorbitol. The arrays were grown for two cycles of 48 hours at 30 °C
1066 in a custom growth and imaging platform (S&P Robotics Inc.), which incubated the plates and
1067 took a picture of each plate every 2 hours.

1068

1069

1070 Analysis of DHFR-PCA of Pbs2 mutants binding to SH3 domain-containing proteins

1071

1072 First, the ImageMagick command line tool (ImageMagick Studio LLC 2023) was used to crop the
1073 images of the selection plates as well as change them to grayscale and invert the colors, using
1074 the commands: convert -colorspace LinearGray, convert -crop 4200X2800+530+320 and convert
1075 -negate. Colony sizes were then quantified using the Python package Pyphe (Kamrad *et al.* 2020),
1076 using the command pyphe-quantify timecourse --grid auto_1536 --t 1 --d 3 --s 0.05. The colony
1077 sizes were analyzed and visualized using a custom script written in R 4.3.1 (R Core Team 2023),
1078 based on a previous analysis (Dionne *et al.* 2021), and using R packages from the tidyverse
1079 collection (Wickham *et al.* 2019). Colony sizes were filtered, and colonies which had not grown at
1080 the end of the diploid selection were removed from the PCA results. Colony sizes were log2
1081 transformed and then normalized to avoid bias from a position in the array or from the plate they
1082 grew on by subtracting the log2-transformed median colony size for each row, column and 1536
1083 array, including the border colonies. Scores were rescaled, so that the median of the scores of
1084 the Sho1 and wild-type Pbs2 interaction was equivalent to 1 and the median of scores of the Sho1
1085 and stuffed Pbs2 interaction was equivalent to 0.

1086

1087 Analysis of contacts in SH3-motif structures

1088 Contacts were analyzed for 4 structures. Sho1-Pbs2 was generated by AlphaFold-Multimer, as
1089 described above. Abp1-Ark (PDB accession 2RPN), Nbp2-Ste20 (PDB accession 2LCS), and
1090 Bem1-2-Ste20 (PDB accession 2RQW) were all previously measured NMR structure ensembles,
1091 composed of the 20 individual structures. All 20 structures were used for determining the contacts,
1092 although only the designated representative structure was used for visualization. The structures
1093 were imported into ChimeraX 1.8 (Pettersen *et al.* 2021), and the ChimeraX “Contacts” tool was
1094 used to detect all pairs of atoms from different proteins with a Van der Waals radius overlap \geq -
1095 0.40 Å. This was done for all atoms in the motif-bearing protein preceding position -3 in the
1096 standard motif numbering. So, in Pbs2, this was done for all atoms in positions 71 to 92
1097 (SNQSEQDKGSSQSPKHIQQIVN), for Ark1 this was done for positions -10 to -4 (KPKLHSP),
1098 and for Ste20 this was done for positions -14 to -4 (SSSANGKFIPS). To identify equivalent
1099 positions in the four SH3 domains which form contacts, the structures of the 4 domains were
1100 aligned using the MUSTANG tool (Konagurthu *et al.* 2006), and a standard numbering was
1101 determined based on this alignment (Table S9). The contacts between atoms were filtered to
1102 simply indicate all contacts between residues, and are summarized in Table S10, using the

1103 aforementioned standard numbering. The minimum distance between residues or proteins was
1104 calculated in a custom R script, using the bio3d package (Grant *et al.* 2006).

1105 Data availability

1106 Strains and plasmids are available upon request. All analysis scripts and visualization scripts are
1107 available on Github at the following address: https://github.com/Landrylab/Jordan_et_al_2024. All
1108 data, including demultiplexed sequencing data, results from the DHFR-PCA experiments, growth
1109 curve data, predicted structures, protein alignments, and all files and information necessary to run
1110 the scripts are available in the following Dryad repository:
1111 <https://doi.org/10.5061/dryad.79cnp5j3z>.

1112
1113

1114 Acknowledgments

1115 The authors thank Philippe C. Després, Moïra Dion and Dan Evans-Yamamoto for help with
1116 sequencing data analysis. We also thank all members of the LandryLab team for thoughtful
1117 comments on the experiments and on figure conception. All molecular graphics were performed
1118 using UCSF ChimeraX 1.8. The protein structure predictions were enabled by computing
1119 resources provided by the Digital Research Alliance of Canada.
1120

1121 Funding

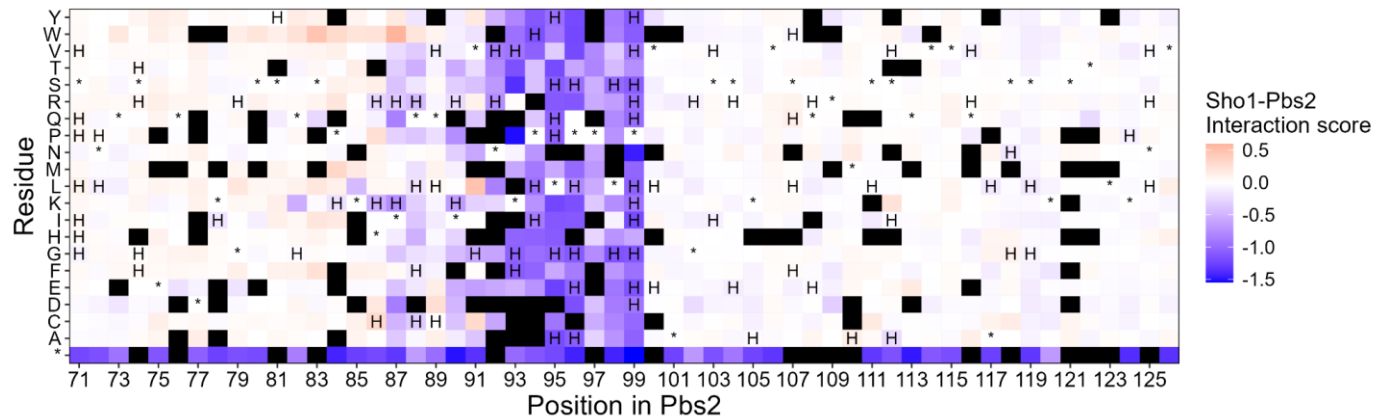
1122 This work was supported by Canadian Institutes of Health Research Foundation grant number
1123 387697 and Human Frontier Science Program research grant RGP34/2018 to CRL. C.R.L. holds
1124 the Canada Research Chair in Cellular Systems and Synthetic Biology. D.J. was supported by
1125 the Canada Graduate Scholarship - Master's program from NSERC, a graduate scholarship from
1126 PROTEO, a graduate scholarship from the NSERC CREATE program EvoFunPath, a
1127 Postgraduate Scholarship - Doctoral from NSERC and a Doctoral scholarship from FRQS. D.B.
1128 was funded by the EMBO Long-Term Fellowship (LTF) (ALTF 1069-2019). U.D. was
1129 funded by an NSERC graduate fellowship.
1130
1131

1132 Author contributions

1133 All authors were involved in the design of the study. C.R.L. supervised this work and obtained
1134 funding. D.J. and A.K.D. performed the experiments. D.J. performed the computational analyses.

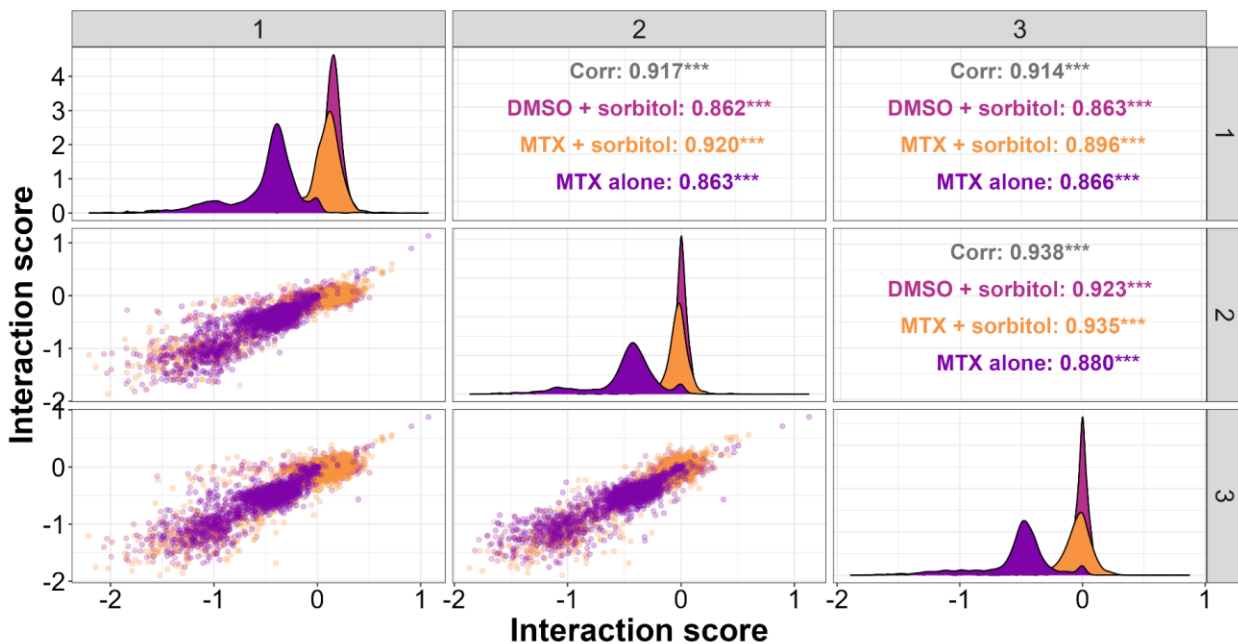
1135 D.J. wrote the first draft of the manuscript. All authors contributed to revising and writing the final
1136 version of the manuscript.
1137
1138
1139

1140 **Supplementary Figures**

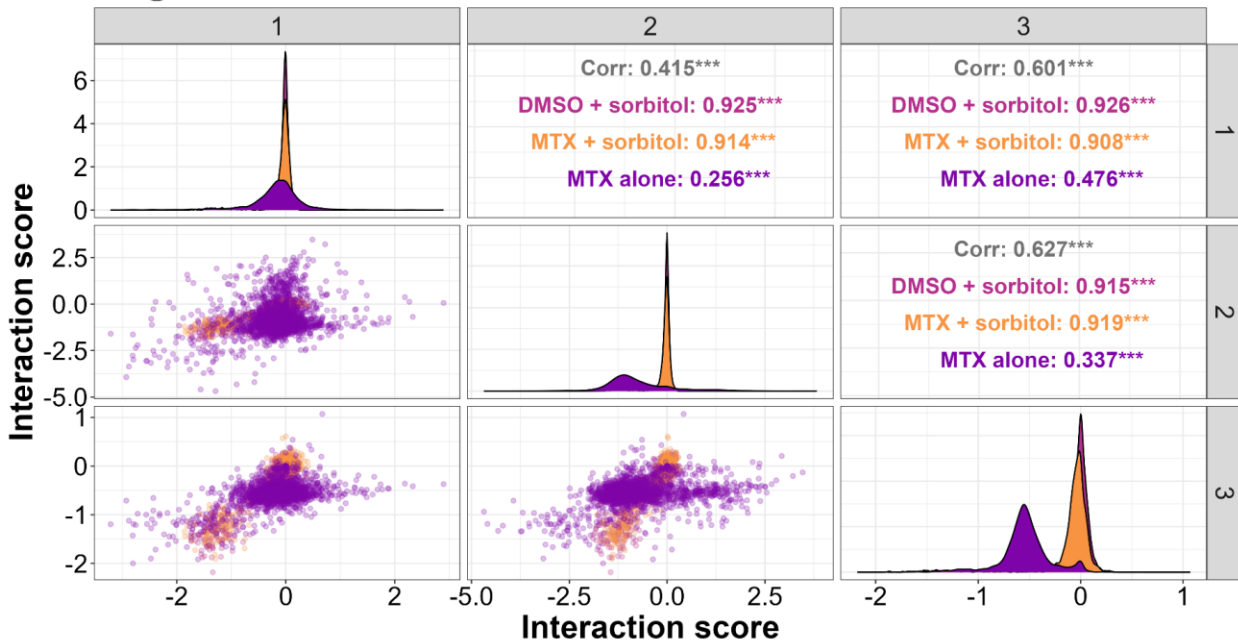


1141
1142 Figure S1.
1143 Sho1-Pbs2 interaction scores for Pbs2 mutants in the DHFR-PCA on the DMS library of the region
1144 surrounding the Pbs2 motif. Scores are indicated for each mutant according to their position in
1145 Pbs2 and the residue that it was mutated to. The wild-type residue for each position is indicated
1146 by an asterisk (*). Mutants which significantly affect the Hog1-Pbs2 interaction are marked with
1147 the letter H (Two-sided Mann-Whitney U test with false discovery rate corrected p-value < 0.05).
1148 Mutants which were removed from the dataset for having too few reads in the initial timepoint are
1149 marked in black. Each measurement is the median of all codons in each replicate coding for the
1150 same residue, with 3 to 18 replicates for each mutant.

a Sho1



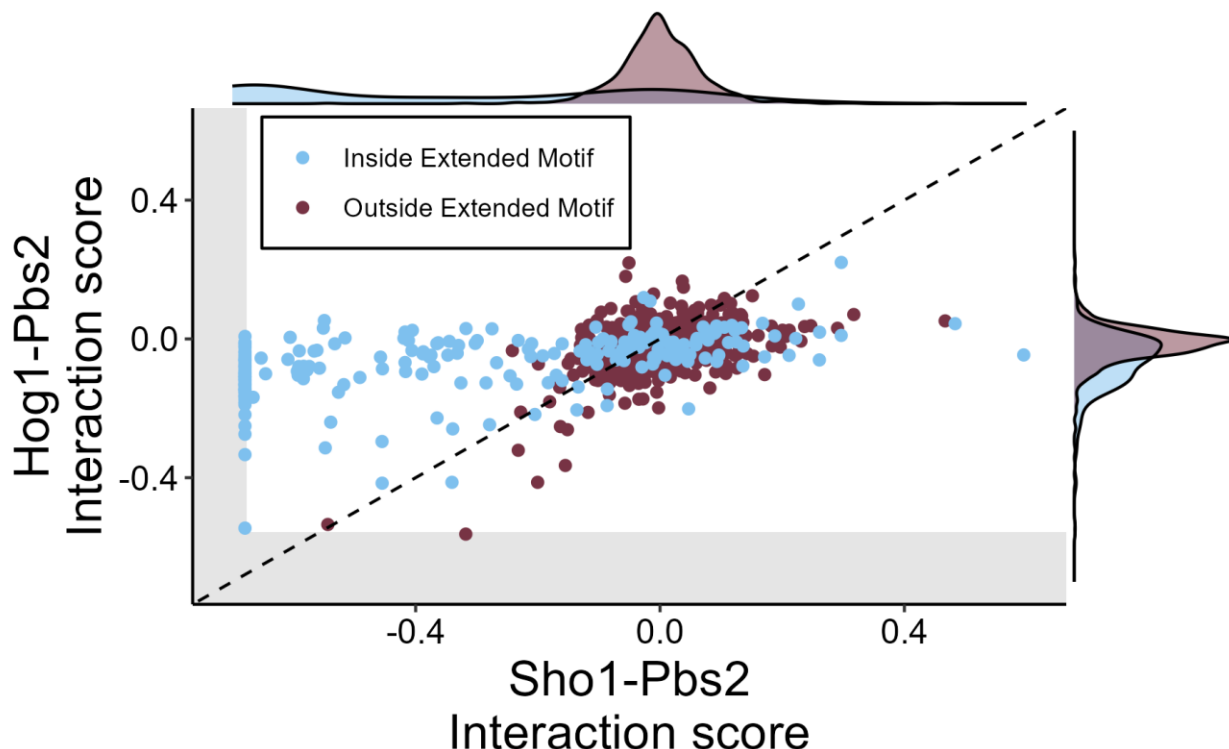
b Hog1



1151
1152

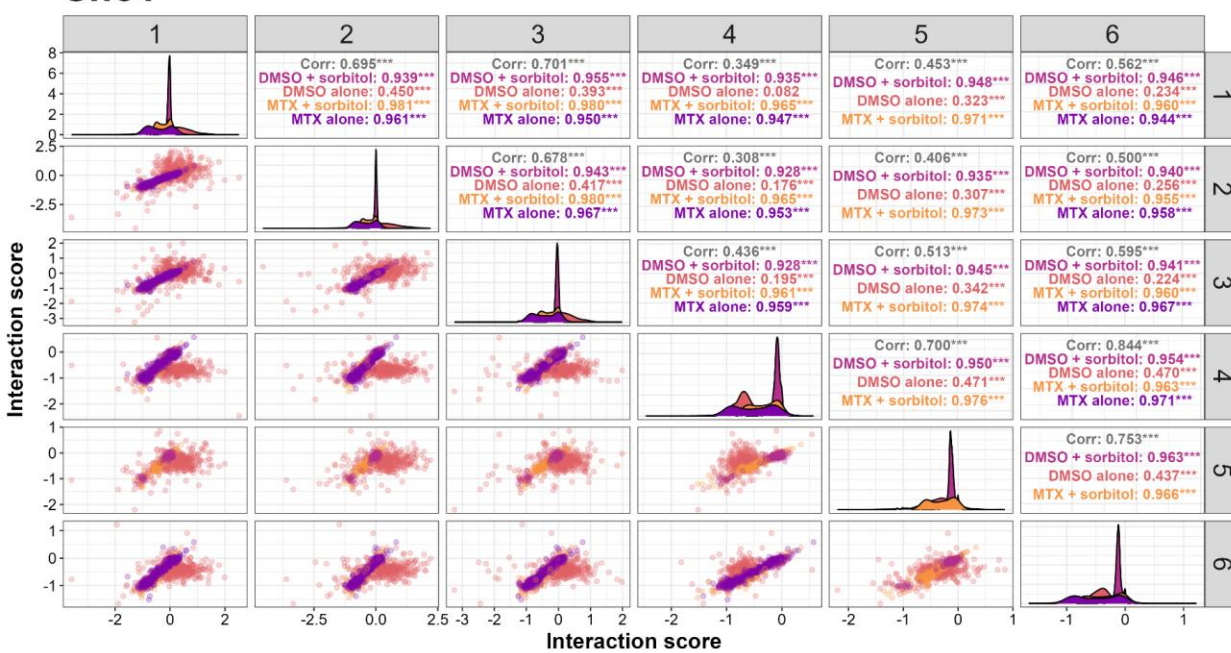
1153 Figure S2.
1154 Correlation between replicates in the DHFR-PCA experiments on DMS libraries surrounding
1155 region of the Pbs2 binding motif a) Scatterplot between the 3 replicates of the Sho1-Pbs2 DHFR-
1156 PCA interaction scores for mutants in the DMS library of the region surrounding the Pbs2 motif.
1157 Each point represents one Pbs2 codon variant in one condition (with or without sorbitol, with MTX
1158 or with only DMSO), as indicated by the color in the corresponding panel on the top right. Pearson
1159 correlations also indicated in the top right panels. In the panels on the diagonal, the distribution

1160 of scores for a given condition and replicate is shown. The replicate number is indicated in the
1161 gray rectangle. b) Scatterplot between the 3 replicates of the Hog1-Pbs2 DHFR-PCA interaction
1162 scores for mutants in the DMS library of the region surrounding the Pbs2 motif. Each point
1163 represents one Pbs2 codon variant in one condition (with or without sorbitol, with MTX or with
1164 only DMSO), as indicated by the color in the corresponding panel on the top right. Pearson
1165 correlations also indicated in the top right panels. In the panels on the diagonal, the distribution
1166 of scores for a given condition and replicate is shown. The replicate number is indicated in the
1167 gray rectangle.
1168

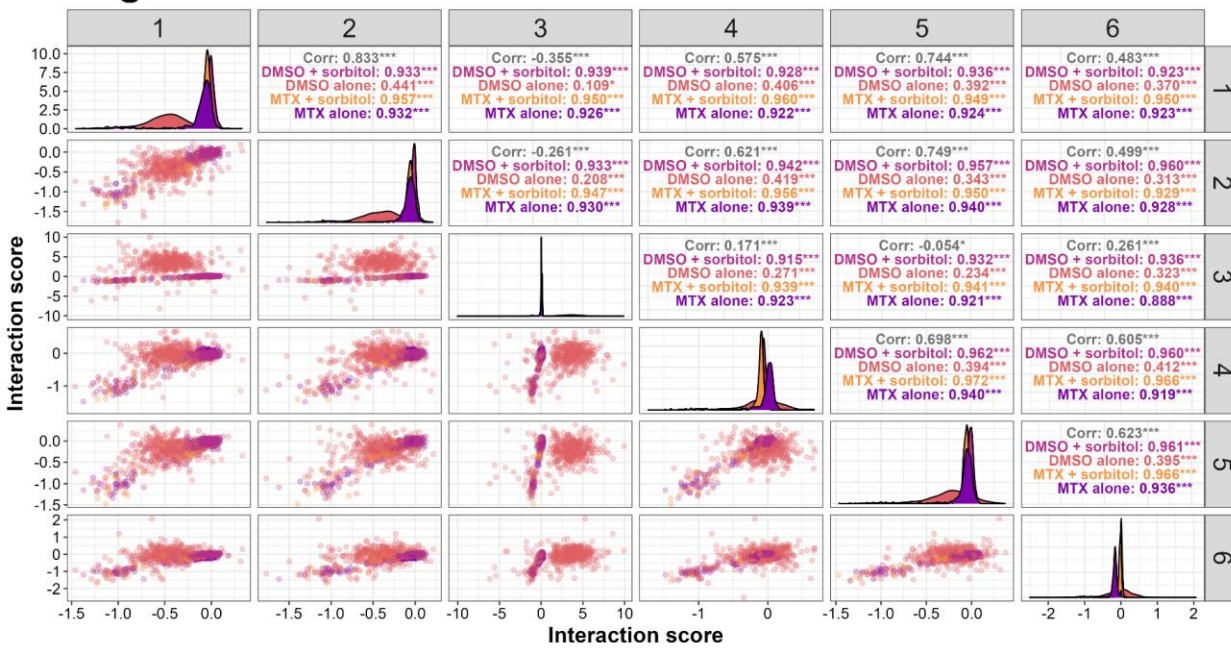


1169
1170
1171
1172 Figure S3.
1173 Scatterplot of interaction scores for missense and silent mutants in the DMS library of the region
1174 surrounding the motif, for the interaction of Pbs2 with either Sho1 or Hog1. Points are colored
1175 according to whether the mutants are situated inside or outside the extended motif. The dotted
1176 line represents the diagonal. The gray rectangles on the left and bottom of the panel represent
1177 the 97.5 percentile of scores for the nonsense variants of Pbs2, which do not express the DHFR
1178 F[3] fragment. As such, they represent the limit of detectable signal in the assay. The points which
1179 have scores comparable to the nonsense mutations, and therefore no detectable interaction, were
1180 placed at the limit of the gray rectangle to indicate that no interaction was detected. In the margins,
1181 density plots show the distribution of scores for mutants situated either inside or outside the
1182 extended motif. Each point represents the median of all codons in each replicate coding for the
1183 same mutation, with 3 to 18 replicates for each mutant.
1184

a Sho1



b Hog1



1185

1186

Figure S4.

1187

Correlation between replicates in the DHFR-PCA experiments on DMS libraries of the extended

1188

Pbs2 binding motif a) Scatterplot between the 6 replicates of the Sho1-Pbs2 DHFR-PCA

1189

interaction scores for mutants in the DMS library of the extended Pbs2 motif. Each point

1190

represents one Pbs2 codon variant in one condition (with or without sorbitol, with MTX or with

1191

only DMSO), as indicated by the color in the corresponding panel on the top right. Pearson

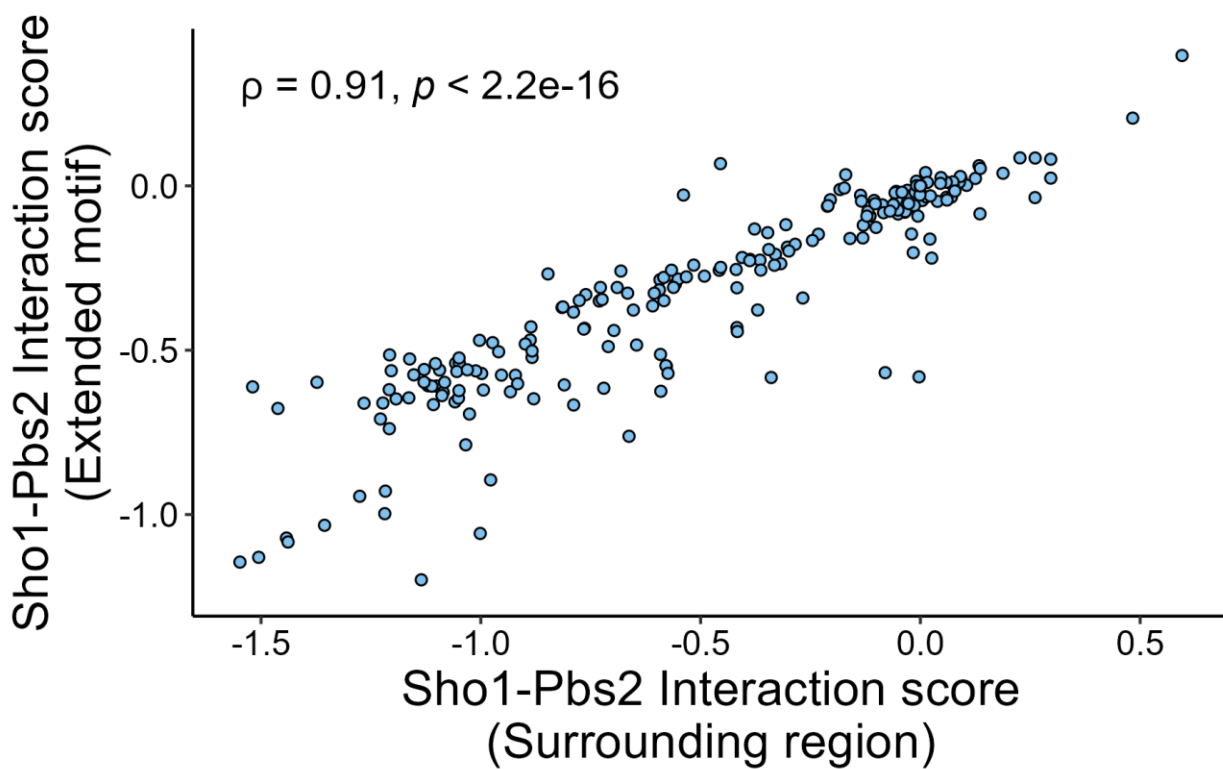
1192

correlations also indicated in the top right panels. In the panels on the diagonal, the distribution

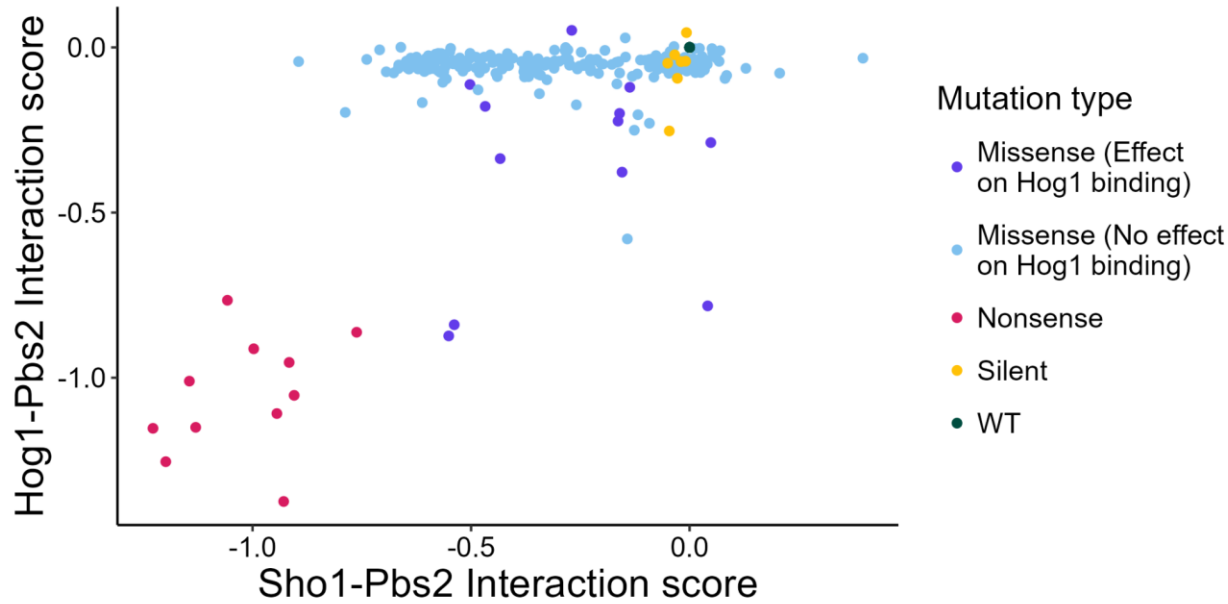
1193

of scores for a given condition and replicate is shown. The replicate number is indicated in the

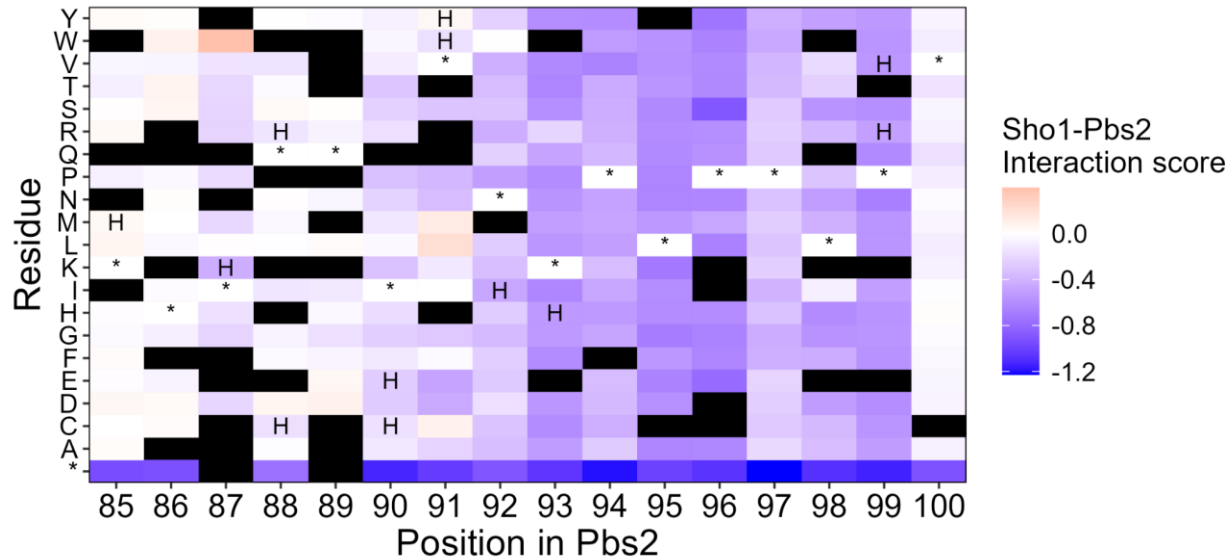
1194 gray rectangle. b) Scatterplot between the 6 replicates of the Hog1-Pbs2 DHFR-PCA interaction
1195 scores for mutants in the DMS library of the extended Pbs2 motif. Each point represents one Pbs2
1196 codon variant in one condition (with or without sorbitol, with MTX or with only DMSO), as indicated
1197 by the color in the corresponding panel on the top right. Pearson correlations also indicated in the
1198 top right panels. In the panels on the diagonal, the distribution of scores for a given condition and
1199 replicate is shown. The replicate number is indicated in the gray rectangle.
1200
1201



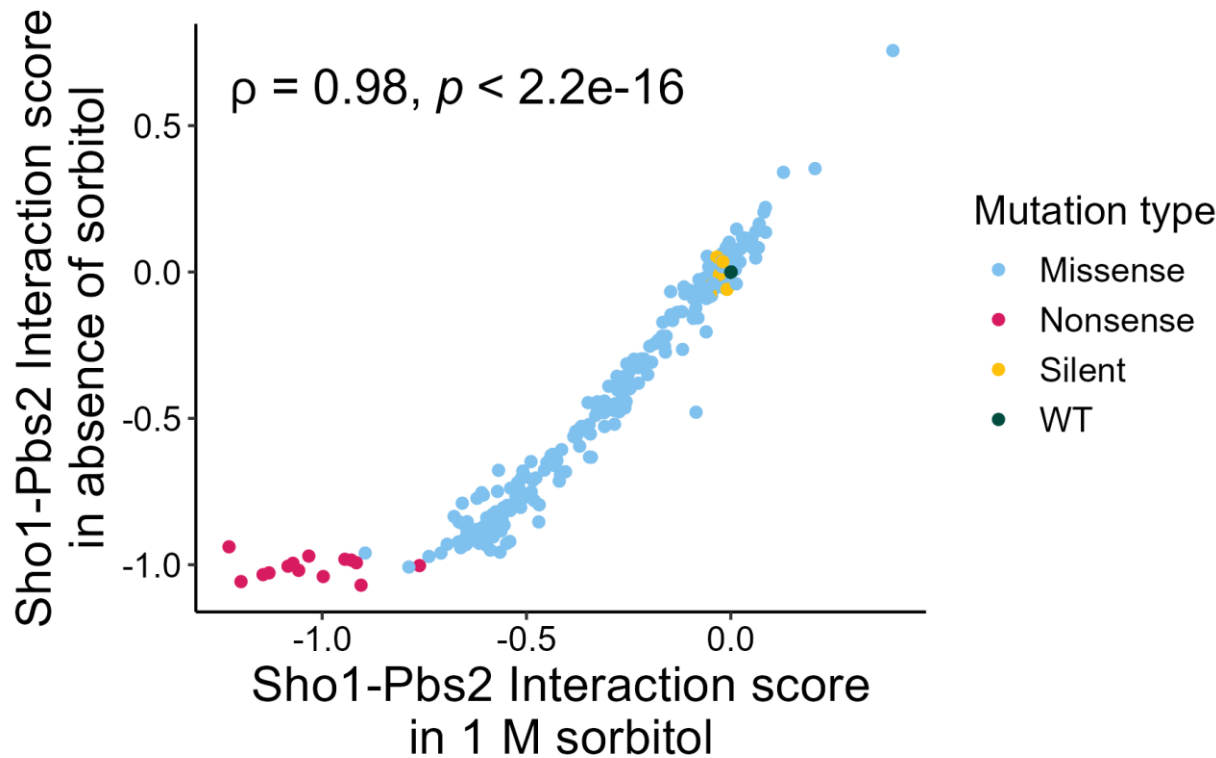
1202
1203 Figure S5.
1204 Scatterplot of interaction scores of Pbs2 mutants in the initial DHFR-PCA screen on the DMS
1205 library of the surrounding region of the motif, and the subsequent DHFR-PCA screen on the DMS
1206 library of only the extended motif (positions 85 to 100). Scores shown were measured in the
1207 presence of methotrexate and 1 M of sorbitol. Each point represents the median of all codons in
1208 each replicate coding for the same mutation, with 3 to 18 replicates for each mutant. Spearman's
1209 rho 0.91, $p < 2.2\text{X}10^{-16}$.
1210
1211
1212
1213



1214
1215
1216 Figure S6.
1217 Scatterplot of interaction scores of the Pbs2 extended motif DMS library mutants with Sho1 and
1218 Hog1, in the presence of 1 M of sorbitol. Purple missense points represent Pbs2 mutants which
1219 have an interaction score with Hog1 which is significantly different to the combination of silent
1220 mutants and wild-type Pbs2 (Two-sided Mann-Whitney U test with false discovery rate corrected
1221 p-value < 0.05), while blue missense points represent mutants for which the Hog1 interaction
1222 score is not significantly different to the combination of silent mutants and wild-type Pbs2. The
1223 combination of silent mutations and wild type represents all mutants expressing the wild-type
1224 protein sequence. Since the Hog1 interaction is used to measure abundance and stability of the
1225 Pbs2 mutants, the significantly different mutants are considered to have an effect on the
1226 abundance or the stability of Pbs2 and were not kept for the remainder of the analysis. The only
1227 exceptions are the nonsense mutants, which were kept because they provide a useful reference.
1228 Each point represents the median of all codons in each replicate coding for the same mutation,
1229 with 3 to 18 replicates for each mutant.
1230
1231
1232
1233
1234

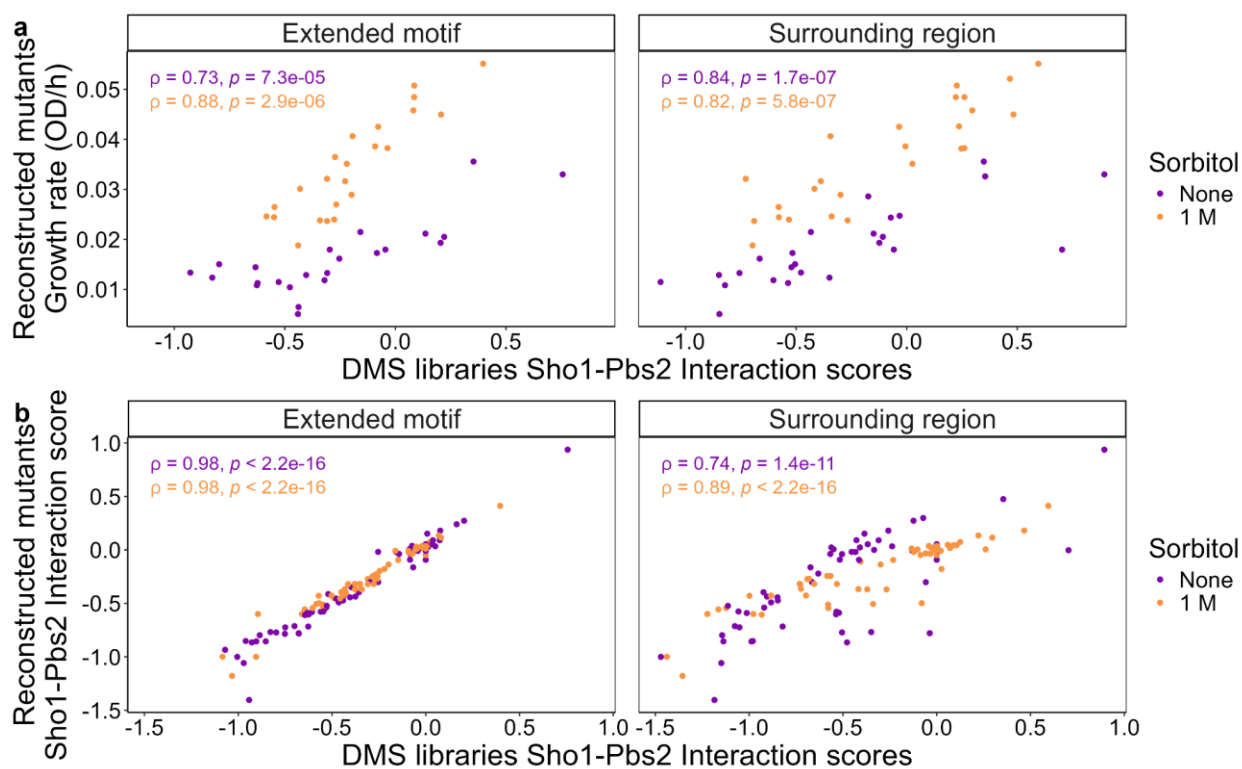


1235
1236 Figure S7.
1237 Sho1-Pbs2 interaction scores for Pbs2 mutants in the DHFR-PCA on the DMS library of the
1238 extended Pbs2 motif. Scores are indicated for each mutant according to their position in Pbs2
1239 and the residue that it was mutated to. The wild-type residue for each position is indicated by an
1240 asterisk (*). Mutants which significantly affect the Hog1-Pbs2 interaction are marked with the letter
1241 H (Two-sided Mann-Whitney U test with false discovery rate corrected p-value < 0.05). Mutants
1242 which were removed from the dataset for having too few reads in the initial timepoint are marked
1243 in black. Each measurement represents the median of all codons in each replicate coding for the
1244 same residue, with 3 to 18 replicates for each mutant.
1245
1246
1247
1248
1249
1250
1251
1252
1253
1254
1255
1256



1257
1258
1259 Figure S8.
1260 Scatterplot of the Sho1 interaction scores for all mutants in the Pbs2 extended motif DMS library,
1261 in the presence and absence of 1 M of sorbitol. Measurements in DHFR-PCA media with
1262 methotrexate. The correlation has a spearman's rho of 0.98, and a p-value $< 2.2 \times 10^{-16}$. The
1263 measurements for the interaction in 1 M sorbitol have a greater range due to the greater activation
1264 of the HOG pathway. Each point represents the median of all codons in each replicate coding for
1265 the same mutation, with 3 to 18 replicates for each mutant.
1266
1267
1268

1269



1270

1271

1272 Figure S9.

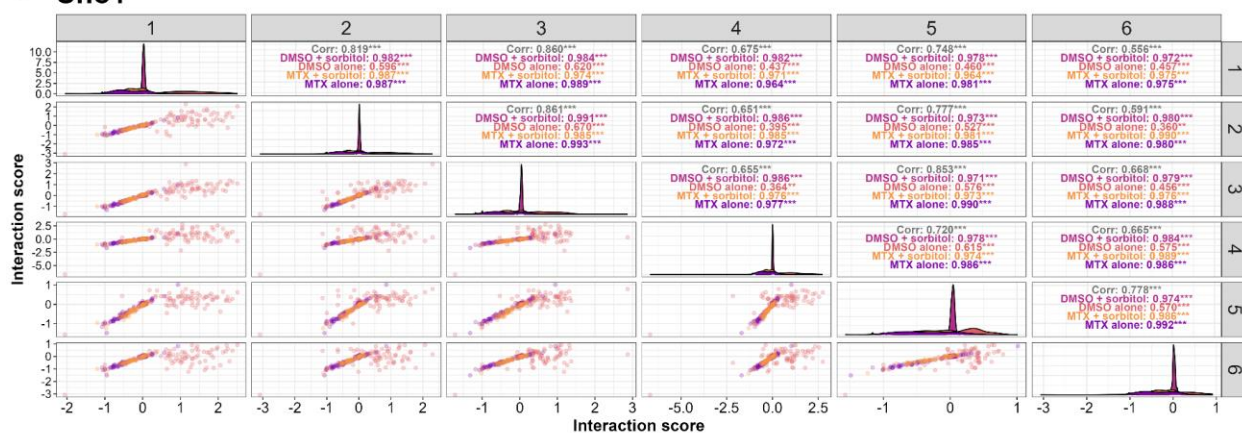
1273 Validation of pooled DHFR-PCA effects by individually reconstructed mutants

1274 a) Scatterplot of Sho1-Pbs2 interaction scores as measured in pooled competition DHFR-PCA of
1275 the DMS libraries (x-axis) and growth rate of the same mutations individually reconstructed, in
1276 DHFR-PCA growth curves (y-axis). Results from the DMS library of the extended motif (left) and
1277 the DMS library of the surrounding region (right), in the presence (orange) or absence (purple) of
1278 1 M of sorbitol. The spearman correlations between the two methods of measuring the interaction
1279 strength are indicated on the plots. The values for the DMS library interaction scores represent
1280 the median of all codons in each replicate coding for the same mutation, with 3 to 18 replicates
1281 for each mutant. The values for the growth rate represent the median of 3 replicates. b) Scatterplot
1282 of Sho1-Pbs2 interaction scores as measured in pooled competition DHFR-PCA of the DMS
1283 libraries (x-axis) and measured in pooled competition DHFR-PCA of individually reconstructed
1284 mutants (y-axis). Results from the DMS library of the extended motif (left) and the DMS library of
1285 the surrounding region (right), in the presence (orange) or absence (purple) of 1 M of sorbitol.
1286 The spearman correlations between the two methods of measuring the interaction strength are
1287 indicated on the plots. The values for the DMS library interaction scores represent the median of
1288 all codons in each replicate coding for the same mutation, with 3 to 18 replicates for each mutant.
1289 The values for the reconstructed mutants represent the median of 3 to 6 replicates.

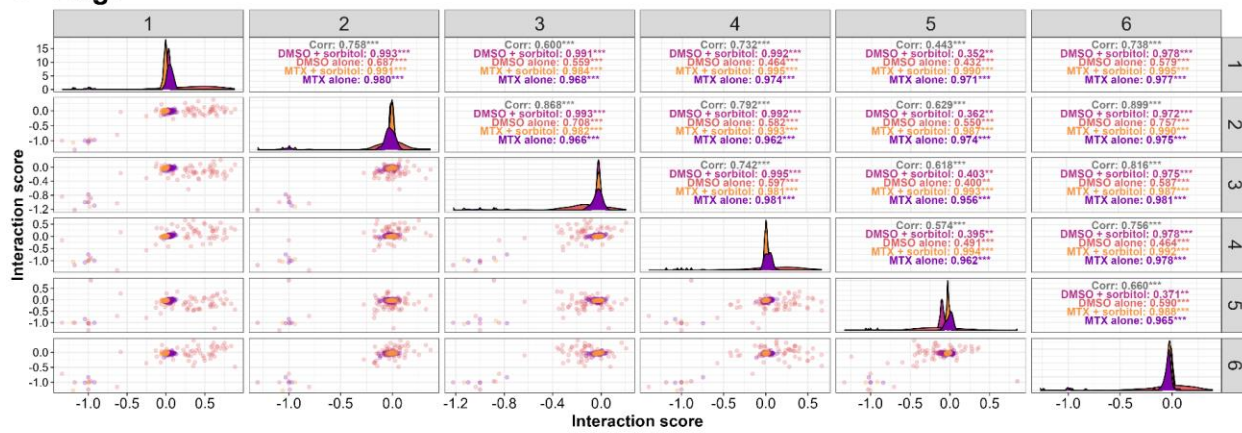
1290

1291

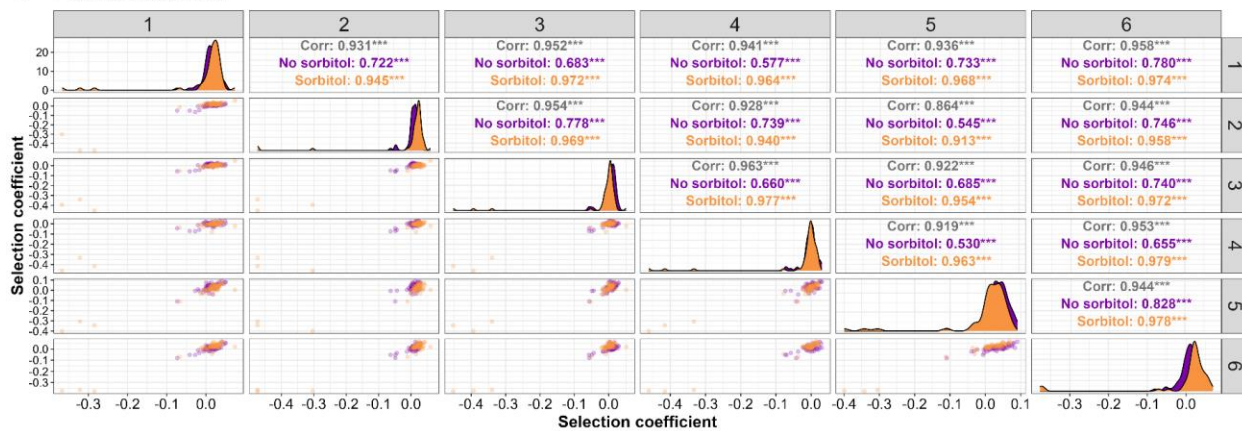
a Sho1



b Hog1



c Proliferation



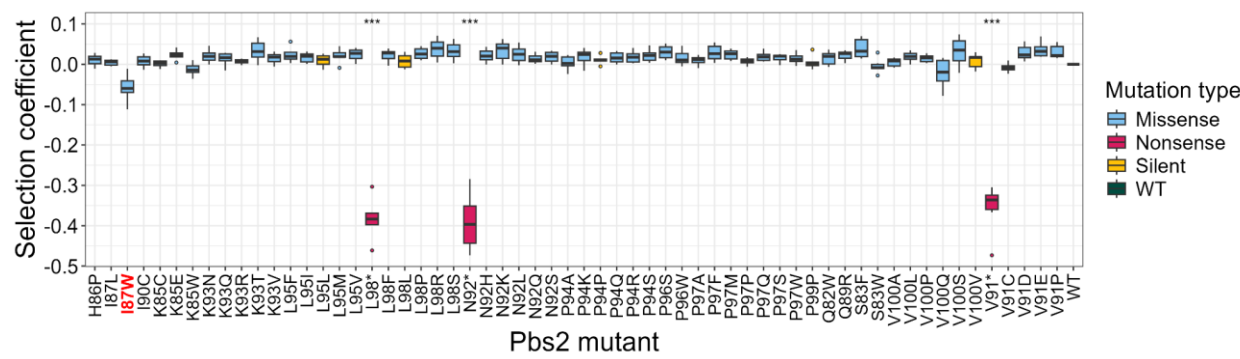
1292

1293 Figure S10.

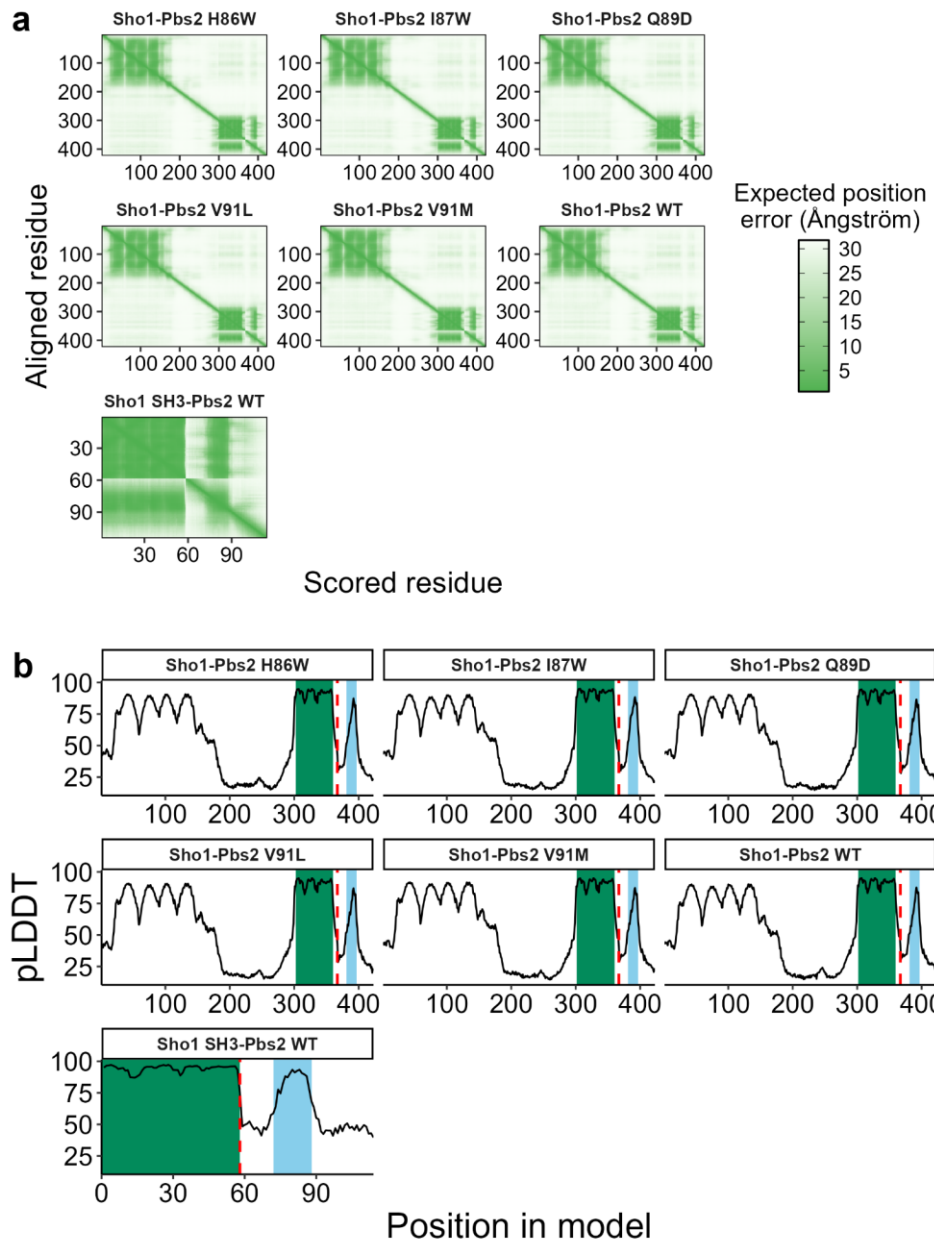
1294 Correlation between replicates in the DHFR-PCA experiments on DMS libraries of the extended
1295 Pbs2 binding motif

1296 a) Scatterplot between the 6 replicates of the Sho1-Pbs2 DHFR-PCA interaction scores for
1297 mutants in the Pbs2 validation DMS library. Each point represents one Pbs2 codon variant in one
1298 condition (with or without sorbitol, with MTX or with only DMSO), as indicated by the color in the
1299 corresponding panel on the top right. Pearson correlations also indicated in the top right panels.

1300 In the panels on the diagonal, the distribution of scores for a given condition and replicate is
1301 shown. The replicate number is indicated in the gray rectangle. b) Scatterplot between the 6
1302 replicates of the Hog1-Pbs2 DHFR-PCA interaction scores for mutants in the Pbs2 validation
1303 DMS library. Each point represents one Pbs2 codon variant in one condition (with or without
1304 sorbitol, with MTX or with only DMSO), as indicated by the color in the corresponding panel on
1305 the top right. Pearson correlations also indicated in the top right panels. In the panels on the
1306 diagonal, the distribution of scores for a given condition and replicate is shown. The replicate
1307 number is indicated in the gray rectangle. c) Scatterplot between the 6 replicates of selection
1308 coefficients for mutants in the Pbs2 validation DMS library measuring cell proliferation. Each point
1309 represents one Pbs2 codon variant in one condition (with or without sorbitol), as indicated by the
1310 color in the corresponding panel on the top right. Pearson correlations also indicated in the top
1311 right panels. In the panels on the diagonal, the distribution of scores for a given condition and
1312 replicate is shown. The replicate number is indicated in the gray rectangle.
1313
1314



1315
1316 Figure S11.
1317 Impact on growth rate measured as selection coefficients for individually reconstructed Pbs2
1318 mutants in SC synthetic media with 1 M sorbitol. The strains contain no DHFR fragments on any
1319 proteins. Boxplots show the distribution of 6 replicates per mutant. The selection coefficient is
1320 normalized by the growth of the wild-type sequence, making the wild-type selection coefficient
1321 zero. Only the 3 nonsense mutants grew significantly less than wild-type Pbs2 and the silent
1322 mutants (Welch's t-test with false discovery rate correction p-value < 0.05), although I87W
1323 (highlighted in red on axis), which is the mutant with the highest Sho1-Pbs2 interaction score
1324 shows a marked decrease in selection coefficient (p-value = 0.066).
1325



1326

1327

Figure S12.

1328

Confidence metrics for the seven structures predicted using AlphaFold2-Multimer. Sho1 SH3-

1329

Pbs2 WT is the structure in figure 2b, Sho1-Pbs2 WT is the structure in figure 3a and 3b, Sho1-

1330

Pbs2 I87W is the structure in figure 3c, and all others are the structures with the same Pbs2

1331

mutants in figure S13. a) Predicted aligned error (PAE) values for the 7 predicted structures,

1332

output from AlphaFold-Multimer. b) pLDDT value for each position in the 7 predicted structures,

1333

output from AlphaFold-Multimer. Positions corresponding to the SH3 domain of Sho1 are

1334

indicated by a green background, and positions corresponding to the extended motif of Pbs2 are

1335

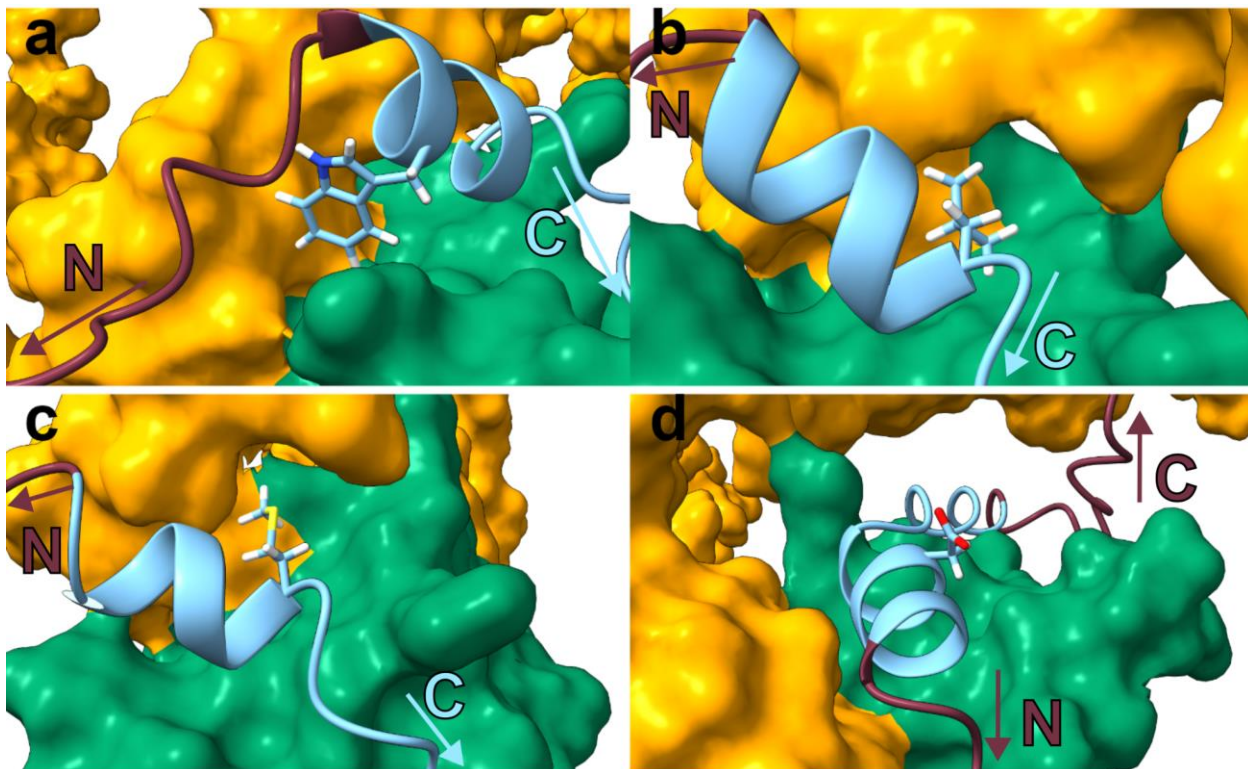
indicated by a blue background. Since AlphaFold-Multimer combines the sequences of both

1336

proteins into a single model, a red dashed line was used to mark the end of the Sho1 portion of

1337

the model, and the beginning of the Pbs2 portion of the model.

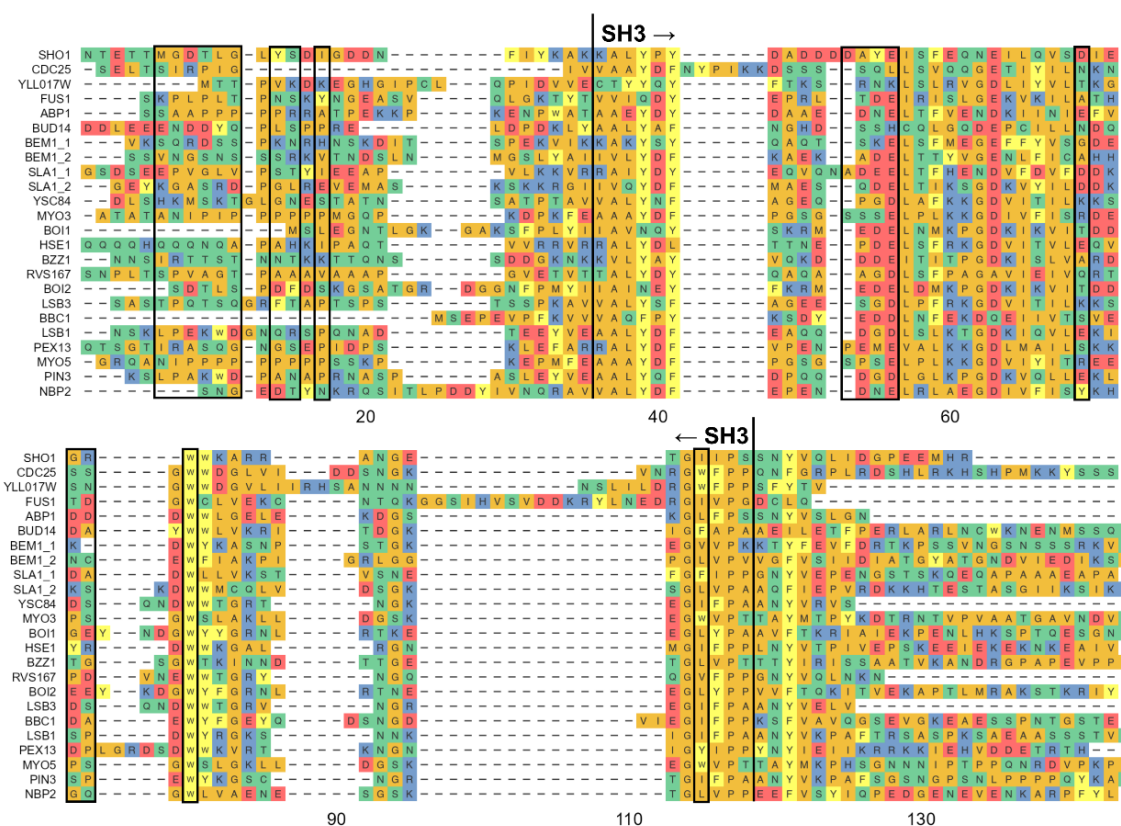


1338
1339
1340
1341
1342
1343
1344
1345
1346
1347

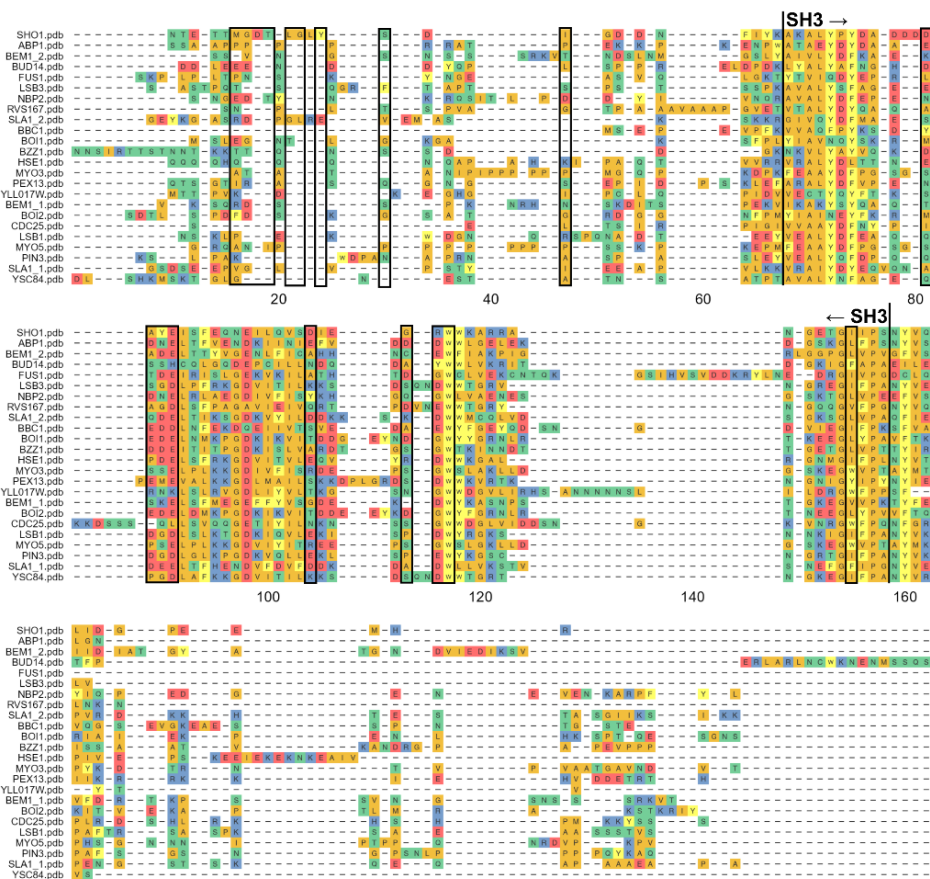
Figure S13.

Close-up details of AlphaFold-Multimer predicted complexes of Sho1 with Pbs2 mutants a) H86W, b) V91L, c) V91M and d) Q89D. The predicted structures are colored as in panel a of figure 3, with the SH3 domain of Sho1 in green, the non-SH3 portions of Sho1 in orange, the extended motif of Pbs2 in light blue and the rest of Pbs2 in burgundy. The side chain of the mutated residue is shown with oxygen atoms in red, nitrogen atoms in dark blue, sulfur atoms in yellow, hydrogen atoms in white and carbon atoms the same color as the extended motif, while all other side chains in Pbs2 are hidden. The orientation of Pbs2 is shown by annotations indicating which end is nearer the N-terminus (N) and which end is nearer the C-terminus (C).

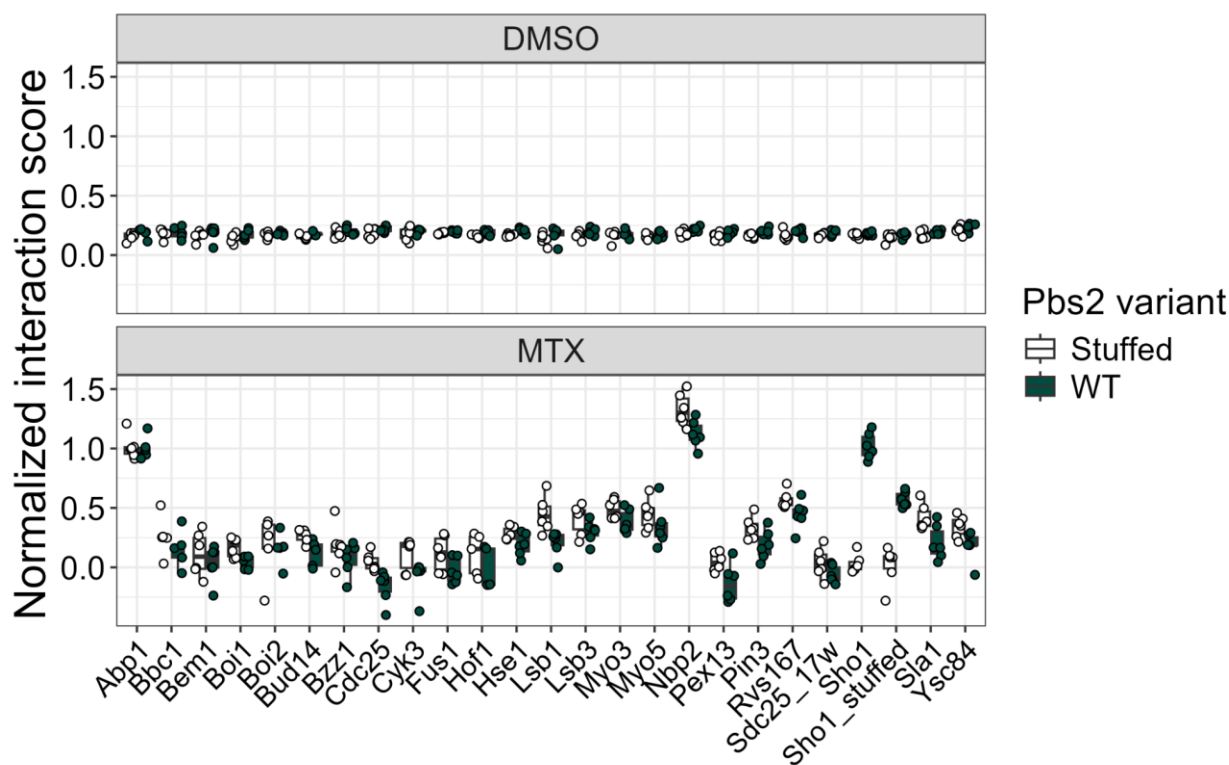
a



b

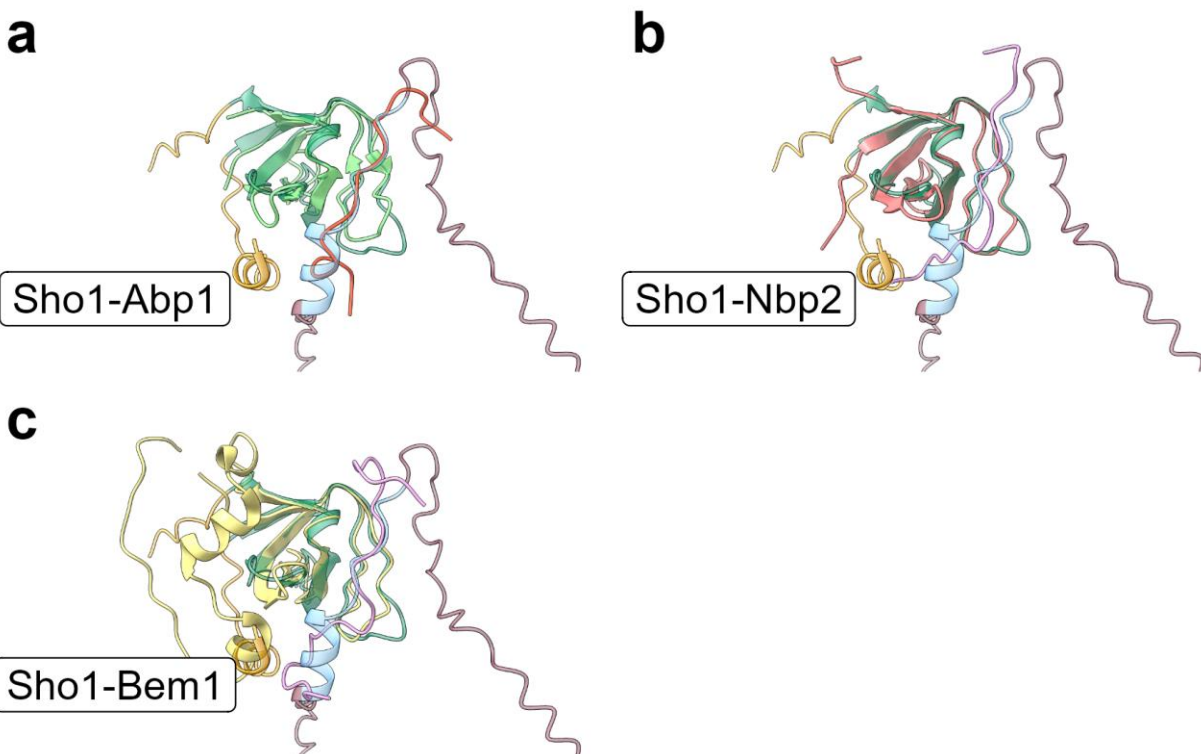


1349 Figure S14.
1350 Sequence and structural alignments of yeast SH3 domains and adjacent sequences a) Multiple
1351 sequence alignment of yeast SH3 domains with 25 residues on each side. Residues which in the
1352 predicted Sho1-Pbs2 structure are within 5 Å of Pbs2 residues situated in the extended motif but
1353 not the canonical motif are surrounded by a black rectangle. Beginning and end of the SH3
1354 domain of Sho1 marked above the alignment. b) Multiple structural alignment of predicted yeast
1355 SH3 domains with 25 residues on each side, from MUSTANG. Residues which in the predicted
1356 Sho1-Pbs2 structure are within 5 Å of Pbs2 residues situated in the extended motif but not the
1357 canonical motif are surrounded by a black rectangle. Beginning and end of the SH3 domain of
1358 Sho1 marked above the alignment.
1359

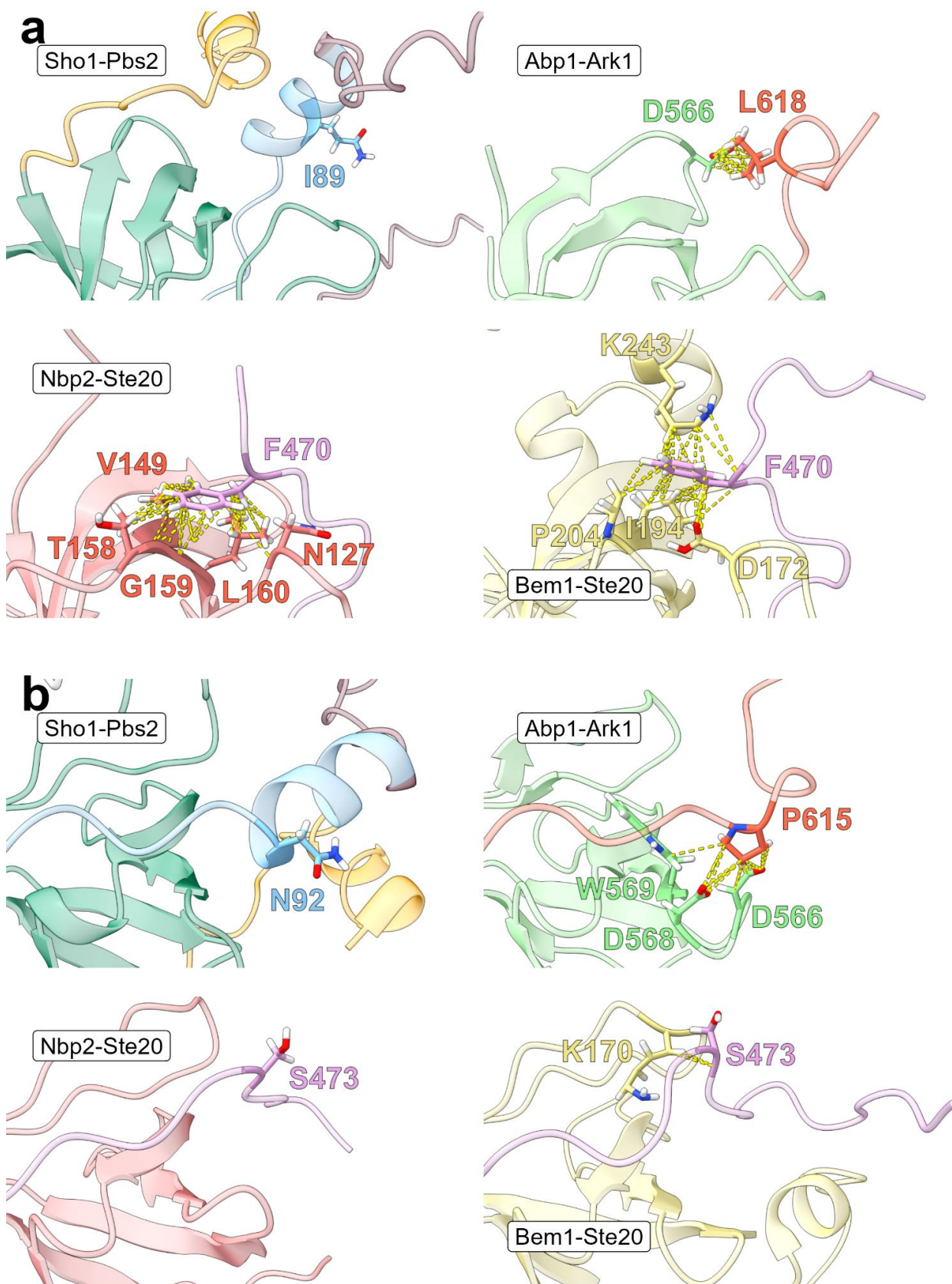


1360
1361
1362 Figure S15.
1363 Interaction score of wild-type Pbs2 (green) or Pbs2 where positions 76 to 126 have been replaced
1364 with a flexible stuffer sequence (Stuffed, white) with all yeast SH3-containing proteins. Controls
1365 grown on DMSO and not MTX, and therefore not measuring the interaction, are shown in the top
1366 panel. All replicates shown as points. Scores normalized with 1 being the median of Sho1 - wild
1367 type Pbs2 interactions and 0 being the median of Sho1 - stuffed Pbs2 interactions. A control
1368 where the SH3 domain of Sho1 was replaced by the same neutral, flexible stuffer sequence used
1369 for Pbs2-stuffed was also included, with the name Sho1_stuffed.

1370



1371
1372 Figure S16.
1373 Predicted structure of the Sho1-Pbs2 interaction superimposed with other SH3-motif pairs. The
1374 Sho1-Pbs2 structure is semi-transparent and colored as in figure 3a, with the SH3 domain of
1375 Sho1 in green, the non-SH3 portions of Sho1 in orange, the Pbs2 extended motif in light blue and
1376 the rest of Pbs2 in burgundy. Sho1-Pbs2 structure was superimposed with the a) Abp1-Ark
1377 structure (Abp1 - light green, Ark1 - pink), b) Nbp2-Ste20 structure (Nbp2 - orange-pink, Ste20 -
1378 light pink), and c) Bem1-2-Ste20 structure (Bem1 - yellow, Ste20 - light pink). Structures were
1379 superimposed using the Chimera X tool “Matchmaker” (Pettersen *et al.* 2021) to minimize root
1380 mean square deviance of backbone atom distances of the SH3 domains with Sho1.
1381



1383 Figure S17.
1384 Additional differing contacts between SH3-extended motif pairs
1385 a) Visualization of the side-chains and contacts of position (-7) in the Sho1-Pbs2 predicted
1386 structure , Abp1-Ark1 structure (PDB accession 2RPN), Nbp2-Ste20 structure (PDB accession
1387 2LCS) and Bem1-Ste20 (PDB accession 2RQW). Sho1-Pbs2 predicted structure colored as in
1388 figure 3a, with the SH3 domain of Sho1 in green, the non-SH3 portions of Sho1 in orange, the
1389 Pbs2 extended motif in light blue and the rest of Pbs2 in burgundy. All four structures were
1390 superimposed using the Chimera X tool “Matchmaker” (Pettersen *et al.* 2021) to minimize root
1391 mean square deviance of backbone atom distances of the SH3 domains with Sho1, then pictures
1392 were captured separately. b) Visualization of the side-chains and contacts of position (-4) of the
1393 same structures as in panel a). All four structures were superimposed using the Chimera X tool
1394 “Matchmaker” (Pettersen *et al.* 2021) to minimize root mean square deviance of backbone atom
1395 distances of the SH3 domains with Sho1, then pictures were captured separately.
1396
1397

1398 Literature cited

- 1399
- 1400 Amberg D., D. C. Burke, and J. N. Strathern, 2005 *Methods in yeast genetics: a Cold Spring*
1401 *Harbor Laboratory course manual*. Cold Spring Harbor Laboratory Press, Cold Spring
1402 Harbor, N.Y.
- 1403 Andrews S., 2010 FastQC: a quality control tool for high throughput sequence data
- 1404 Attali D., and C. Baker, 2023 *ggExtra: Add Marginal Histograms to “ggplot2”, and More “ggplot2”*
1405 *Enhancements*.
- 1406 Bendel A. M., A. J. Faure, D. Klein, K. Shimada, R. Lyautey, *et al.*, 2024 The genetic
1407 architecture of protein interaction affinity and specificity. Nat. Commun. 15: 8868.
- 1408 Bolger A. M., M. Lohse, and B. Usadel, 2014 Trimmomatic: a flexible trimmer for Illumina
1409 sequence data. Bioinformatics 30: 2114–2120.
- 1410 Bult C. J., and P. W. Sternberg, 2023 The alliance of genome resources: transforming
1411 comparative genomics. Mamm. Genome 34: 531–544.

- 1412 Dalgarno D. C., M. C. Botfield, and R. J. Rickles, 1997 SH3 domains and drug design: Ligands,
1413 structure, and biological function. *Pept. Sci.* 43: 383–400.
- 1414 Davey N. E., G. Travé, and T. J. Gibson, 2011 How viruses hijack cell regulation. *Trends
1415 Biochem. Sci.* 36: 159–169.
- 1416 Delplace V., A. Ortín-Martínez, E. L. S. Tsai, A. N. Amin, V. Wallace, *et al.*, 2019 Controlled
1417 release strategy designed for intravitreal protein delivery to the retina. *J. Control. Release*
1418 293: 10–20.
- 1419 Després P. C., A. F. Cisneros, E. M. M. Alexander, R. Sonigara, C. Gagné-Thivierge, *et al.*,
1420 2022 Asymmetrical dose responses shape the evolutionary trade-off between antifungal
1421 resistance and nutrient use. *Nat Ecol Evol* 6: 1501–1515.
- 1422 Dibyachintan S., A. K. Dube, D. Bradley, P. Lemieux, U. Dionne, *et al.*, 2024 Cryptic genetic
1423 variation shapes the fate of gene duplicates in a protein interaction network. *bioRxiv*
1424 2024.02.23.581840.
- 1425 Dionne U., É. Bourgault, A. K. Dubé, D. Bradley, F. J. M. Chartier, *et al.*, 2021 Protein context
1426 shapes the specificity of SH3 domain-mediated interactions *in vivo*. *Nat. Commun.* 12:
1427 1597.
- 1428 Dionne U., L. J. Percival, F. J. M. Chartier, C. R. Landry, and N. Bisson, 2022 SRC homology 3
1429 domains: multifaceted binding modules. *Trends Biochem. Sci.* 47: 772–784.
- 1430 Diss G., and B. Lehner, 2018 The genetic landscape of a physical interaction. *eLife* 7.
1431 <https://doi.org/10.7554/eLife.32472>
- 1432 Douangamath A., F. V. Filipp, A. T. J. Klein, P. Barnett, P. Zou, *et al.*, 2002 Topography for
1433 Independent Binding of α -Helical and PPII-Helical Ligands to a Peroxisomal SH3 Domain.

- 1434 Mol. Cell 10: 1007–1017.
- 1435 Dubé A. K., R. Dandage, S. Dibyachintan, U. Dionne, P. C. Després, *et al.*, 2022 Deep
1436 Mutational Scanning of Protein–Protein Interactions Between Partners Expressed from
1437 Their Endogenous Loci In Vivo, pp. 237–259 in *Yeast Functional Genomics: Methods and*
1438 *Protocols*, edited by Devaux F. Springer US, New York, NY.
- 1439 Ernst A., D. Gfeller, Z. Kan, S. Seshagiri, P. M. Kim, *et al.*, 2010 Coevolution of PDZ domain-
1440 ligand interactions analyzed by high-throughput phage display and deep sequencing. Mol.
1441 Biosyst. 6: 1782–1790.
- 1442 Evans R., M. O'Neill, A. Pritzel, N. Antropova, A. Senior, *et al.*, 2022 Protein complex prediction
1443 with AlphaFold-Multimer. bioRxiv 2021.10.04.463034.
- 1444 Faure A. J., J. Domingo, J. M. Schmiedel, C. Hidalgo-Carcedo, G. Diss, *et al.*, 2022 Mapping
1445 the energetic and allosteric landscapes of protein binding domains. Nature 604: 175–183.
- 1446 Feng S., C. Kasahara, R. J. Rickles, and S. L. Schreiber, 1995 Specific interactions outside the
1447 proline-rich core of two classes of Src homology 3 ligands. Proc. Natl. Acad. Sci. U. S. A.
1448 92: 12408–12415.
- 1449 Ferrigno P., F. Posas, D. Koepp, H. Saito, and P. A. Silver, 1998 Regulated nucleo/cytoplasmic
1450 exchange of HOG1 MAPK requires the importin beta homologs NMD5 and XPO1. EMBO J.
1451 17: 5606–5614.
- 1452 Fowler D. M., and S. Fields, 2014 Deep mutational scanning: a new style of protein science.
1453 Nat. Methods 11: 801–807.
- 1454 Freschi L., F. Torres-Quiroz, A. K. Dubé, and C. R. Landry, 2013 qPCA: a scalable assay to
1455 measure the perturbation of protein-protein interactions in living cells. Mol. Biosyst. 9: 36–

- 1456 43.
- 1457 Gaußmann S., R. Peschel, J. Ott, K. M. Zak, J. Sastre, *et al.*, 2024 Modulation of peroxisomal
1458 import by the PEX13 SH3 domain and a proximal FxxxF binding motif. *Nat. Commun.* 15:
1459 3317.
- 1460 Gorelik M., and A. R. Davidson, 2012 Distinct peptide binding specificities of Src homology 3
1461 (SH3) protein domains can be determined by modulation of local energetics across the
1462 binding interface. *J. Biol. Chem.* 287: 9168–9177.
- 1463 Gouw M., S. Michael, H. Sámano-Sánchez, M. Kumar, A. Zeke, *et al.*, 2018 The eukaryotic
1464 linear motif resource – 2018 update. *Nucleic Acids Res.* 46: D428–D434.
- 1465 Grant B. J., A. P. C. Rodrigues, K. M. ElSawy, J. A. McCammon, and L. S. D. Caves, 2006
1466 Bio3d: an R package for the comparative analysis of protein structures. *Bioinformatics* 22:
1467 2695–2696.
- 1468 Gueldener U., J. Heinisch, G. J. Koehler, D. Voss, and J. H. Hegemann, 2002 A second set of
1469 loxP marker cassettes for Cre-mediated multiple gene knockouts in budding yeast. *Nucleic
1470 Acids Res.* 30: e23.
- 1471 Harris C. R., K. J. Millman, S. J. van der Walt, R. Gommers, P. Virtanen, *et al.*, 2020 Array
1472 programming with NumPy. *Nature* 585: 357–362.
- 1473 Haslam N. J., and D. C. Shields, 2012 Peptide-Binding Domains: Are Limp Handshakes Safest?
1474 *Sci. Signal.* 5: e40–pe40.
- 1475 Hunter J. D., 2007 Matplotlib: A 2D Graphics Environment. *Comput. Sci. Eng.* 9: 90–95.
- 1476 Illumina, Nextera DNA Indexes. Illumina Support Docs.

- 1477 ImageMagick Studio LLC, 2023 *ImageMagick*.
- 1478 Ivarsson Y., and P. Jemth, 2019 Affinity and specificity of motif-based protein-protein
1479 interactions. *Curr. Opin. Struct. Biol.* 54: 26–33.
- 1480 Jumper J., R. Evans, A. Pritzel, T. Green, M. Figurnov, *et al.*, 2021 Highly accurate protein
1481 structure prediction with AlphaFold. *Nature* 596: 583–589.
- 1482 Kamrad S., M. Rodríguez-López, C. Cotobal, C. Correia-Melo, M. Ralser, *et al.*, 2020 Pyphe, a
1483 python toolbox for assessing microbial growth and cell viability in high-throughput colony
1484 screens. *eLife* 9. <https://doi.org/10.7554/eLife.55160>
- 1485 Kaneko T., L. Li, and S. S.-C. Li, 2008 The SH3 domain--a family of versatile peptide- and
1486 protein-recognition module. *Front. Biosci.* 13: 4938–4952.
- 1487 Kaneko T., H. Huang, X. Cao, X. Li, C. Li, *et al.*, 2012 Superbinder SH2 Domains Act as
1488 Antagonists of Cell Signaling. *Sci. Signal.* 5: ra68–ra68.
- 1489 Karlsson O. A., G. N. Sundell, E. Andersson, Y. Ivarsson, and P. Jemth, 2016 Improved affinity
1490 at the cost of decreased specificity: a recurring theme in PDZ-peptide interactions. *Sci.*
1491 *Rep.* 6: 34269.
- 1492 Kassambara A., 2020 *ggpubr*: “ggplot2” Based Publication Ready Plots
- 1493 Kassambara A., 2021 *rstatix*: Pipe-Friendly Framework for Basic Statistical Tests
- 1494 Katoh K., and D. M. Standley, 2013 MAFFT multiple sequence alignment software version 7:
1495 improvements in performance and usability. *Mol. Biol. Evol.* 30: 772–780.
- 1496 Kazlauskas A., C. Schmotz, T. Kesti, J. Hepojoki, I. Kleino, *et al.*, 2016 Large-Scale Screening
1497 of Preferred Interactions of Human Src Homology-3 (SH3) Domains Using Native Target

- 1498 Proteins as Affinity Ligands. Mol. Cell. Proteomics 15: 3270–3281.
- 1499 Keck F., 2020 Handling biological sequences in R with the bioseq package. Methods Ecol. Evol.
1500 11: 1728–1732.
- 1501 Kelil A., E. D. Levy, and S. W. Michnick, 2016 Evolution of domain-peptide interactions to
1502 coadapt specificity and affinity to functional diversity. Proc. Natl. Acad. Sci. U. S. A. 113:
1503 E3862–E3871.
- 1504 Kelil A., B. Dubreuil, E. D. Levy, and S. W. Michnick, 2017 Exhaustive search of linear
1505 information encoding protein-peptide recognition. PLoS Comput. Biol. 13: e1005499.
- 1506 Kijima Y., D. Evans-Yamamoto, H. Toyoshima, and N. Yachie, 2023 A universal sequencing
1507 read interpreter. Sci Adv 9: eadd2793.
- 1508 Konagurthu A. S., J. C. Whisstock, P. J. Stuckey, and A. M. Lesk, 2006 MUSTANG: a multiple
1509 structural alignment algorithm. Proteins 64: 559–574.
- 1510 Kumar M., S. Michael, J. Alvarado-Valverde, A. Zeke, T. Lazar, *et al.*, 2024 ELM-the Eukaryotic
1511 Linear Motif resource-2024 update. Nucleic Acids Res. 52: D442–D455.
- 1512 Kursula P., I. Kursula, Y. H. Song, K. Paraskevopoulos, and M. Wilmanns, 2008 YEAST SHO1
1513 SH3 DOMAIN COMPLEXED WITH A PEPTIDE FROM PBS2
- 1514 Langmead B., C. Trapnell, M. Pop, and S. L. Salzberg, 2009 Ultrafast and memory-efficient
1515 alignment of short DNA sequences to the human genome. Genome Biol. 10: R25.
- 1516 Lee C. H., K. Saksela, U. A. Mirza, B. T. Chait, and J. Kuriyan, 1996 Crystal structure of the
1517 conserved core of HIV-1 Nef complexed with a Src family SH3 domain. Cell 85: 931–942.
- 1518 Lemieux P., D. Bradley, A. K. Dubé, U. Dionne, and C. R. Landry, 2024 Dissection of the role of

- 1519 a Src homology 3 domain in the evolution of binding preference of paralogous proteins.
- 1520 Genetics 226. <https://doi.org/10.1093/genetics/iyad175>
- 1521 Li S. S.-C., 2005 Specificity and versatility of SH3 and other proline-recognition domains:
- 1522 structural basis and implications for cellular signal transduction. Biochem. J 390: 641–653.
- 1523 Liao T.-J., H. Jang, R. Nussinov, and D. Fushman, 2020 High-affinity interactions of the
- 1524 nSH3/cSH3 domains of Grb2 with the C-terminal proline-rich domain of SOS1. J. Am.
- 1525 Chem. Soc. 142: 3401–3411.
- 1526 Lim W. A., F. M. Richards, and R. O. Fox, 1994 Structural determinants of peptide-binding
- 1527 orientation and of sequence specificity in SH3 domains. Nature 372: 375–379.
- 1528 Maeda T., M. Takekawa, and H. Saito, 1995 Activation of Yeast PBS2 MAPKK by MAPKKKs or
- 1529 by Binding of an SH3-Containing Osmosensor. Science 269: 554–558.
- 1530 Mapes J., and I. M. Ota, 2004 Nbp2 targets the Ptc1-type 2C Ser/Thr phosphatase to the HOG
- 1531 MAPK pathway. EMBO J. 23: 302–311.
- 1532 Marles J. A., S. Dahesh, J. Haynes, B. J. Andrews, and A. R. Davidson, 2004 Protein-Protein
- 1533 Interaction Affinity Plays a Crucial Role in Controlling the Sho1p-Mediated Signal
- 1534 Transduction Pathway in Yeast. Mol. Cell 14: 813–823.
- 1535 Martin M., 2011 Cutadapt removes adapter sequences from high-throughput sequencing reads.
- 1536 EMBnet.journal 17: 10–12.
- 1537 Masella A. P., A. K. Bartram, J. M. Truszkowski, D. G. Brown, and J. D. Neufeld, 2012
- 1538 PANDAseq: paired-end assembler for illumina sequences. BMC Bioinformatics 13: 31.
- 1539 Messing J., 1983 [2] New M13 vectors for cloning, pp. 20–78 in *Methods in Enzymology*,
- 1540 Academic Press.

- 1541 Michnick S. W., E. D. Levy, C. R. Landry, J. Kowarzyk, and V. Messier, 2016 The Dihydrofolate
1542 Reductase Protein-Fragment Complementation Assay: A Survival-Selection Assay for
1543 Large-Scale Analysis of Protein–Protein Interactions. *Cold Spring Harb. Protoc.* 2016:
1544 db.prot090027.
- 1545 Miyazaki K., 2011 Chapter seventeen - MEGAWHOP Cloning: A Method of Creating Random
1546 Mutagenesis Libraries via Megaprimer PCR of Whole Plasmids, pp. 399–406 in *Methods in*
1547 *Enzymology, Synthetic Biology, Part B*. edited by Voigt C. Academic Press.
- 1548 Monera O. D., T. J. Sereda, N. E. Zhou, C. M. Kay, and R. S. Hodges, 1995 Relationship of
1549 sidechain hydrophobicity and alpha-helical propensity on the stability of the single-stranded
1550 amphipathic alpha-helix. *J. Pept. Sci.* 1: 319–329.
- 1551 Morgan M., and T. Nguyen, *AlphaMissenseR*.
- 1552 Murakami Y., K. Tatebayashi, and H. Saito, 2008 Two adjacent docking sites in the yeast Hog1
1553 mitogen-activated protein (MAP) kinase differentially interact with the Pbs2 MAP kinase
1554 kinase and the Ptp2 protein tyrosine phosphatase. *Mol. Cell. Biol.* 28: 2481–2494.
- 1555 Pawson T., M. Raina, and P. Nash, 2002 Interaction domains: from simple binding events to
1556 complex cellular behavior. *FEBS Lett.* 513: 2–10.
- 1557 Paysan-Lafosse T., M. Blum, S. Chuguransky, T. Grego, B. L. Pinto, *et al.*, 2023 InterPro in
1558 2022. *Nucleic Acids Res.* 51: D418–D427.
- 1559 Pettersen E. F., T. D. Goddard, C. C. Huang, E. C. Meng, G. S. Couch, *et al.*, 2021 UCSF
1560 ChimeraX: Structure visualization for researchers, educators, and developers. *Protein Sci.*
1561 30: 70–82.
- 1562 Posas F., and H. Saito, 1997 Osmotic Activation of the HOG MAPK Pathway via Ste11p

- 1563 MAPKKK: Scaffold Role of Pbs2p MAPKK. *Science* 276: 1702–1705.
- 1564 R Core Team, 2023 *R: A Language and Environment for Statistical Computing*. R Foundation
1565 for Statistical Computing, Vienna, Austria.
- 1566 Rice P., I. Longden, and A. Bleasby, 2000 EMBOSS: the European Molecular Biology Open
1567 Software Suite. *Trends Genet.* 16: 276–277.
- 1568 Rickles R. J., M. C. Botfield, X. M. Zhou, P. A. Henry, J. S. Brugge, *et al.*, 1995 Phage display
1569 selection of ligand residues important for Src homology 3 domain binding specificity. *Proc.*
1570 *Natl. Acad. Sci. U. S. A.* 92: 10909–10913.
- 1571 Robles J. T., H. J. Lou, G. Shi, P. L. Pan, and B. E. Turk, 2023 Linear motif specificity in
1572 signaling through p38 α and ERK2 mitogen-activated protein kinases. *Proceedings of the*
1573 *National Academy of Sciences* 120: e2316599120.
- 1574 Rochette S., G. Diss, M. Filteau, J.-B. Leducq, A. K. Dubé, *et al.*, 2015 Genome-wide protein-
1575 protein interaction screening by protein-fragment complementation assay (PCA) in living
1576 cells. *J. Vis. Exp.* <https://doi.org/10.3791/52255>
- 1577 Rognes T., T. Flouri, B. Nichols, C. Quince, and F. Mahé, 2016 VSEARCH: a versatile open
1578 source tool for metagenomics. *PeerJ* 4: e2584.
- 1579 Ryan O. W., S. Poddar, and J. H. D. Cate, 2016 CRISPR-Cas9 Genome Engineering in
1580 *Saccharomyces cerevisiae* Cells. *Cold Spring Harb. Protoc.* 2016.
1581 <https://doi.org/10.1101/pdb.prot086827>
- 1582 Saito H., and F. Posas, 2012 Response to Hyperosmotic Stress. *Genetics* 192: 289–318.
- 1583 Schloerke B., D. Cook, J. Larmarange, F. Briatte, M. Marbach, *et al.*, 2023 *GGally: Extension to*
1584 “*ggplot2*.”

- 1585 Slowikowski K., 2023 *ggrepel: Automatically Position Non-Overlapping Text Labels with*
1586 *"ggplot2."*
- 1587 Stein A., and P. Aloy, 2008 Contextual specificity in peptide-mediated protein interactions. PLoS
1588 One 3: e2524.
- 1589 Stollar E. J., B. Garcia, P. A. Chong, A. Rath, H. Lin, *et al.*, 2009 Structural, functional, and
1590 bioinformatic studies demonstrate the crucial role of an extended peptide binding site for
1591 the SH3 domain of yeast Abp1p. *J. Biol. Chem.* 284: 26918–26927.
- 1592 Takaku T., K. Ogura, H. Kumeta, N. Yoshida, and F. Inagaki, 2010 Solution structure of a novel
1593 Cdc42 binding module of Bem1 and its interaction with Ste20 and Cdc42. *J. Biol. Chem.*
1594 285: 19346–19353.
- 1595 Tarassov K., V. Messier, C. R. Landry, S. Radinovic, M. M. S. Molina, *et al.*, 2008 An in Vivo
1596 Map of the Yeast Protein Interactome. *Science* 320: 1465–1470.
- 1597 Tatebayashi K., K. Yamamoto, K. Tanaka, T. Tomida, T. Maruoka, *et al.*, 2006 Adaptor
1598 functions of Cdc42, Ste50, and Sho1 in the yeast osmoregulatory HOG MAPK pathway.
1599 *EMBO J.* 25: 3033–3044.
- 1600 The pandas development team, 2023 *pandas-dev/pandas: Pandas*.
- 1601 Tonikian R., X. Xin, C. P. Toret, D. Gfeller, C. Landgraf, *et al.*, 2009 Bayesian Modeling of the
1602 Yeast SH3 Domain Interactome Predicts Spatiotemporal Dynamics of Endocytosis
1603 Proteins. *PLoS Biol.* 7: e1000218.
- 1604 Van Roey K., B. Uyar, R. J. Weatheritt, H. Dinkel, M. Seiler, *et al.*, 2014 Short Linear Motifs:
1605 Ubiquitous and Functionally Diverse Protein Interaction Modules Directing Cell Regulation.
1606 *Chem. Rev.* 114: 6733–6778.

- 1607 Varadi M., S. Anyango, M. Deshpande, S. Nair, C. Natassia, *et al.*, 2022 AlphaFold Protein
1608 Structure Database: massively expanding the structural coverage of protein-sequence
1609 space with high-accuracy models. *Nucleic Acids Res.* 50: D439–D444.
- 1610 Vincentelli R., K. Luck, J. Poirson, J. Polanowska, J. Abdat, *et al.*, 2015 Quantifying domain-
1611 ligand affinities and specificities by high-throughput holdup assay. *Nat. Methods* 12: 787–
1612 793.
- 1613 Wang C.-H., P. Mehta, and C. J. Bashor, 2018 The strength of protein-protein interactions
1614 controls the information capacity and dynamical response of signaling networks. *bioRxiv*
1615 469197.
- 1616 Wickham H., M. Averick, J. Bryan, W. Chang, L. D. McGowan, *et al.*, 2019 Welcome to the
1617 tidyverse. *Journal of Open Source Software* 4: 1686.
- 1618 Wilke C. O., 2020 cowplot: Streamlined Plot Theme and Plot Annotations for “ggplot2”
- 1619 Yu H., J. K. Chen, S. Feng, D. C. Dalgarno, A. W. Brauer, *et al.*, 1994 Structural basis for the
1620 binding of proline-rich peptides to SH3 domains. *Cell* 76: 933–945.
- 1621 Zarin T., and B. Lehner, 2024 A complete map of specificity encoding for a partially fuzzy
1622 protein interaction. *bioRxiv* 2024.04.25.591103.
- 1623 Zarrinpar A., S.-H. Park, and W. A. Lim, 2003 Optimization of specificity in a cellular protein
1624 interaction network by negative selection. *Nature* 426: 676–680.
- 1625 Zarrinpar A., R. P. Bhattacharyya, M. P. Nittler, and W. A. Lim, 2004 Sho1 and Pbs2 Act as
1626 Coscaffolds Linking Components in the Yeast High Osmolarity MAP Kinase Pathway. *Mol.*
1627 *Cell* 14: 825–832.
- 1628

1629